

1 **The density of ambient black carbon retrieved by a new method:**  
2 **implications to CCN prediction**

删除了: Variations of the

删除了: importance

3  
4 **Jingye Ren<sup>1,2</sup>, Fang Zhang<sup>2\*</sup>, Lu Chen<sup>1</sup>, Jieyao Liu<sup>1</sup>**

5  
6 <sup>1</sup>*College of Global Change and Earth System Science, Beijing Normal University,*  
7 *Beijing 100875, China*

8 <sup>2</sup>*Shenzhen Key Laboratory of Organic Pollution Prevention and Control, School of*  
9 *Civil and Environmental Engineering, Harbin Institute of Technology (Shenzhen),*  
10 *518055 Shenzhen, China*

删除了: <sup>2</sup>School

11 \_\_\_\_\_  
12  
13  
14  
15  
16  
17 **\*Correspondence to: Fang Zhang ([zhangfang2021@hit.edu.cn](mailto:zhangfang2021@hit.edu.cn))**  
18  
19  
20  
21  
22  
23  
24

28 **Abstract.**

29 The effective density of black carbon (BC) is a crucial factor relevant to its aging  
30 degree that would add uncertainty in evaluating its climate effect. Here, we have  
31 developed a new method to retrieve the effective density of internally mixed BC in the  
32 atmosphere combining field observations conducted on 15 November -14 December  
33 2016 in urban Beijing with the Köhler theory. The uncertainty of the retrieval method  
34 was evaluated within  $\pm 30\%$ , which is primarily caused by assumptions of the  
35 hygroscopic parameter of organics and the fraction of primary organic aerosols in non-  
36 hygroscopic or hygroscopic mode. Using the method, we obtain that the ambient  
37 internally-mixed BC, accounting for  $80\pm 20\%$  of total BC aerosol particles, is retrieved  
38 with campaign mean density of  $1.1\pm 0.6\text{ g cm}^{-3}$  during the observed periods. The  
39 retrieved result is comparable with that reported in the literatures. By applying a lower  
40 ( $0.14\text{ g cm}^{-3}$ ) and upper ( $2.1\text{ g cm}^{-3}$ ) limit of the retrieved BC density in cloud  
41 condensation nuclei (CCN) number concentrations ( $N_{\text{CCN}}$ ) estimation, we derived that  
42 neglect of such variations in BC density, led to an uncertainty of  $-28\% \sim 11\%$  in  
43 predicting  $N_{\text{CCN}}$  at supersaturations of  $0.23\%$  and  $0.40\%$ . We also find that the  $N_{\text{CCN}}$  is  
44 more sensitive to the variations of BC density when it is  $< 1.0\text{ g cm}^{-3}$ . This illustrates a  
45 necessity of accounting for the effect of BC density on CCN activity closer to source  
46 regions where the BC particles are mostly freshly emitted. The CCN closure achieves  
47 when introducing the retrieved real-time BC density and mixing state. This study  
48 provides a unique way of utilizing field measurements to infer ambient BC density and

删除了: morphology and mixing state

删除了: develop

删除了: ambient

删除了: new

删除了: new

删除了: BC density during the campaign varies widely from  $0.14$  to  $2.1\text{ g cm}^{-3}$ , with a campaign mean density of  $1.11\pm 0.54\text{ g cm}^{-3}$  for

删除了: that accounts

删除了:  $79\pm 18$

删除了: .

删除了: values fall within the range of typical density of internally-mixed BC

删除了: We further examined the sensitivity of

删除了: prediction to

删除了: of

删除了: , showing

删除了: calculating

删除了: 2

删除了:  $4\%$  by varying the BC density within the retrieved ranges.

删除了: , illustrating

删除了: such

72 highlights the importance of applying variable BC density values in models when  
73 predicting CCN and assessing its relevant climate effect.

删除了: varying

## 74 1 Introduction

75 Black carbon (BC) aerosols, as the major absorber of solar radiation, play a vital  
76 role in energy budget and climate of the earth-atmosphere system by affecting the  
77 radiative forcing and cloud properties (Flanner et al., 2007; Ramanathan and  
78 Carmichael, 2008). The light-absorbing capability induced by BC is related to its  
79 density and morphology (Zhang et al., 2008; Rissler et al., 2014), which can be  
80 modified after mixing with other atmospheric aerosol particles (Khalizov et al., 2009;  
81 Xue et al., 2009). Changes in its physicochemical properties would also regulate its  
82 ability to serve as cloud condensation nuclei (CCN) and further indirectly affect the  
83 radiative balance by affecting the clouds process (Yuan et al., 2008; Wang et al., 2011).  
84 Owing to the complex evolution of the mixing state, density and morphology of BC,  
85 the contribution of BC particles to CCN budgets is still not well understood.

删除了: capability of

删除了: understand

86 BC particles, with diesel vehicles, industrial and residential coal combustion as  
87 major sources, are ubiquitous in urban environments (Bond et al., 2013; Dameto et al.,  
88 2017; Li et al., 2017; Liu et al., 2019a). The mixing state of BC describes the  
89 distribution of the bare BC and coating masteries among the aerosol population.  
90 Typically, freshly generated BC exists in the form of chain aggregates and initially  
91 uncoated, which is known as externally mixed BC (Ex-BC). When the BC particles  
92 were emitted, they generally mix with other materials by condensation, coagulation,

删除了: D.

删除了: 2019).

删除了: . While after aging,

99 and other processes (Riemer et al., 2004; Zhang et al., 2008; Liu et al., 2013; Zhang et  
100 al., 2020a), forming the internally mixed BC (In-BC) particles consisting of BC core  
101 and other chemical components (Cheng et al., 2006; Zhang et al., 2016). The BC  
102 structure would be more compact with regular shapes (Pagels et al., 2009; Zhang et al.,  
103 2008; Wang et al., 2017), and the effective density of internally mixed BC are changed  
104 accordingly with the reconstruction (Liu et al., 2019b). The density and morphology of  
105 BC particles are closely related to its sources, mobility size, coating thickness, coating  
106 material and its chemical composition (Zhang et al., 2008; Pagels et al., 2009; Peng et  
107 al., 2016; Zhang et al., 2022). A wide range of BC density has been reported in previous  
108 studies (Lide 1992; Mccurry et al., 2002; Park et al., 2004; Kiselev et al., 2010). Recent  
109 field measurements have indicated that the average BC density is  $\sim 1.2 \text{ g cm}^{-3}$  in the  
110 ambient atmosphere (Zhang et al., 2016). Field measurements have also indicated that  
111 a considerable fraction of externally mixed/uncoated BC exists (Clarke et al., 2004;  
112 Cheng et al., 2012), although a higher proportion of internally mixed/aged BC particles  
113 in the ambient atmosphere were observed (Schwarz et al., 2008; Massoli et al., 2015;  
114 Chen et al., 2020). In climate models, the BC was generally assumed completely  
115 internally-mixed and treated to have a void-free spherical structure and a density value  
116 of  $1.8 \text{ g cm}^{-3}$  (Bond et al., 2013). This may lead to bias in estimating the climate effect  
117 driven by BC.

118 Previous study based on a case study show that when the aging degree of ambient  
119 particles is low, the BC density ( $\sim 1.8 \text{ g cm}^{-3}$ ) under the spherical assumption will lead  
120 to the overestimation of particle hygroscopicity by 40-50 % and the overestimation can

删除了: 2020). The structure of BC

删除了: H.

删除了: 2019

删除了: after aging

删除了: of BC

删除了: ; Chen et al., 2020) and even

删除了: than that internal/

删除了: ). While, in

删除了: effects

删除了: particles

131 be explained almost 100 % using the effective density of fresh BC ( $\sim 0.45 \text{ g cm}^{-3}$ ) (Fan  
132 et al. 2020). This indicates the importance of using reasonable BC density values in the  
133 calculation of particle hygroscopicity. In addition, when estimating the CCN number  
134 concentration, a significant bias of  $-35 \% \sim +20 \%$  was found due to the assumption of  
135 particle mixing state (Ren et al., 2018). However, these studies have not yet accounted  
136 for such impact of BC density and mixing state on CCN prediction due to lack of real  
137 time measurement data.

删除了: by

删除了: caused by

删除了: account

138 The mixing state and the density of BC particles are usually directly measured by  
139 several techniques, such as an integrated system of a volatility tandem differential  
140 mobility analyzer and a single particle soot photometer (VTDMA-SP2) (Zhang et al.,  
141 2016), or a differential mobility analyzer with a SP2 (DMA-SP2) (Olfert et al., 2007;  
142 Rissler et al., 2014; Wu et al., 2019), and a differential mobility analyzer–centrifugal  
143 particle analyzer–single-particle soot photometer (DMA–CPMA–SP2) system (Liu et  
144 al., 2019b; Yu et al., 2020), etc. However, such techniques or measurements are not  
145 available in many previously conducted field campaigns. In this study, we develop a  
146 novel method for retrieving the mixing state and effective density of ambient BC  
147 particles by combining field measured hygroscopic growth factor and aerosol chemical  
148 composition and Köhler theory (Petters and Kreidenweis, 2007). The uncertainty of the  
149 new retrieval method was evaluated. The retrieved results were also compared and  
150 validated with existing observations. In addition, the effect of BC density and mixing  
151 state on prediction of CCN number concentrations is further evaluated through a  
152 sensitivity and closure test by accounting for the retrieved real-time variations of BC

删除了: H.

删除了: 2019

158 density and mixing state.

## 159 **2 Field measurements and methodology**

### 160 **2.1 Field measurements**

161 Measurements in this study were conducted from 15 November to 14 December  
162 2016 at a typical urban site of Beijing (39.97°N, 116.37°E, 49 m above sea level). The  
163 site locates at the Institute of Atmospheric Physics, Chinese Academy of Sciences,  
164 which is mainly influenced by the surrounding cooking, road traffic and residential coal  
165 burning emissions during the home heating periods (Sun et al., 2016). The detailed  
166 information about the sampling site was presented in previous studies (Sun et al., 2015;  
167 Zhang et al., 2019). The number concentration of condensation nuclei (CN) at each size  
168 was measured by a scanning mobility particle sizer, which is equipped with a  
169 differential mobility analyzer (DMA; model 3081, TSI) and a condensation particle  
170 counter (CPC; model 3772, TSI). ~~Subsequently,~~ the mono-dispersed particles were  
171 introduced into a Droplet Measurement Technologies CCN counter (CCNc, DMT;  
172 Lance et al., 2006) to measure CCN number concentration. A hygroscopic tandem  
173 differential mobility analyzer (HTDMA) system was used to measure the hygroscopic  
174 growth factor (Gf) (Tan et al., 2013). Here, four diameters of 40, 80, 110, 150, and 200  
175 nm are selected in the campaign. Gf is defined as the ratio of the mobility diameter at  
176 the given RH to the dry diameter (Petters and Kreidenweis, 2007). The nonrefractory  
177 submicron aerosol chemical composition was measured by an ~~Aerodyne high-~~  
178 ~~resolution time-of-flight aerosol mass spectrometer (HR-AMS; Xu et al., 2019),~~

删除了: Then

删除了: Aerosol Chemical Speciation Monitor (ACSM; Sun et al., 2015

182 including sulfate, nitrate, ammonium, chloride, and organics. Two factors, including a  
183 non-hygroscopic primary organic aerosol (POA) and hygroscopic secondary organic  
184 aerosol (SOA) were classified by positive matrix factorization (PMF) with PMF  
185 algorithm (v4.2) method (Paatero and Tapper, 1994) and followed the procedures  
186 reported in Ulbrich et al. (2009). The refractory black carbon mass loading was  
187 measured by an aethalometer (model AE33, Magee Scientific Corporation). Both the  
188 nonrefractory materials and BC mass concentration were measured with diameters <  
189 1.0  $\mu\text{m}$ . The detailed description of the instrument operation and data process have been  
190 described in details elsewhere (Ren et al., 2018; Xu et al., 2019; Zhang et al., 2019; Fan  
191 et al., 2020).

删除了: using

删除了: ..

删除了: ..

## 192 2.2 Retrieving the mixing state and density of BC

### 193 2.2.1 Retrieving the mixing state of BC

194 The Gf probability distribution function (Gf-PDF) for a specified diameter can be  
195 retrieved firstly based on the TDMAinv algorithm (Gysel et al., 2009). The  $\kappa$ -PDF can  
196 be further calculated based on the Gf-PDF (Fan et al., 2020). Size-resolved  $\kappa$  is derived  
197 using  $\kappa$ -Köhler theory based on hygroscopic growth factor (Gf) (Petters and  
198 Kreidenweis, 2007),

$$199 \quad \kappa_{gf} = (Gf^3 - 1) \cdot \left[ \frac{1}{RH} \exp\left(\frac{4\sigma_{s/a}M_w}{RT\rho_w D_d Gf}\right) - 1 \right] \quad (1)$$

200 where Gf is hygroscopic growth factor, RH is the relative humidity in the HTDMA  
201 (90 %),  $D_d$  is the dry diameter,  $\sigma_{s/a}$  is assumed to be the surface tension of pure water,

205  $R$  is the universal gas constant,  $T$  is the temperature,  $M_w$  and  $\rho_w$  is the molecular mass,  
 206 and the density of water, respectively.

207 The  $\kappa$ -PDF patterns of particles in different sizes always present two modes: nearly  
 208 hydrophobic (NH) mode with  $\kappa_{gf} \leq 0.1$  and more hygroscopic (MH) mode with  $\kappa_{gf} > 0.1$   
 209 (Fig. S1). Firstly, based on the  $\kappa$ -PDF patterns, the number fraction (NF) of the total  
 210 nearly hydrophobic group with the boundary of  $[0, 0.1]$  was calculated according to the  
 211 following equation:

$$212 \quad NF = \int_0^{0.1} c(\kappa, D_p) d\kappa \quad (2)$$

213 here, the  $\kappa$ -PDF, represented by  $c(\kappa, D_p)$ , was normalized as  $\int c(\kappa, D_p) d\kappa = 1$ , where  
 214  $\kappa$  can be replaced by  $\kappa_{gf}$ ,  $D_p$  is the selected electrical mobility diameter in the campaign.

215 The nearly hydrophobic mode consists of both externally mixed POA (Ex-POA or  
 216 bare POA) and externally mixed BC (Ex-BC). Since the number fraction of the nearly-  
 217 hydrophobic POA would change with the emission and aging processes, in this study,  
 218 we have applied different values for the number fractions of hydrophobic POA (NH-  
 219 POA) under clean (91 %), moderately polluted (70 %), and heavily polluted conditions  
 220 (31 %) by referring the literature (Liu et al., 2021a), as shown in Fig. S2. The number  
 221 concentration of Ex-BC was then calculated using the total number fraction of NH  
 222 mode minus the number of NH-POA.

$$223 \quad N_{POA-containing} = N_{total} \times NF_{POA-containing}$$

$$224 \quad N_{bare-POA} = N_{POA-containing} \times NF_{bare-POA}$$

$$225 \quad N_{Ex-BC} = N_{NH} - N_{bare-POA} \quad (3)$$

226 where  $N_{POA-containing}$  and  $NF_{POA-containing}$  are the number concentration and fraction of

删除了: by using

删除了: Here

删除了: Considering the

删除了: external

删除了: Here,

删除了: POA in

删除了:

删除了: mode ( $NF_{NH-POA}$ ) was assumed to be 70 % according to the simultaneous measurements (Liu et al., 2021), and the rest 30 % of POA is assumed mixed

删除了: other hygroscopic aerosols. And thus,

删除了: fraction



239 POA-containing particles,  $N_{\text{total}}$  is the total number concentration,  $N_{\text{bare-POA}}$  and  $N_{\text{bare-}}$   
240 POA are the number concentration and fraction of bare POA particles, and  $N_{\text{NH}}$  is the  
241 number of nearly- hydrophobic group.

删除了: NH-POA. Then, the

242 The number size distribution of the externally mixed BC ( $n_{\text{EX-BC}}(\log D_p)$ ) can be  
243 calculated based on the particle number size distribution (PNSD) and the number  
244 fraction of the hydrophobic mode of BC ( $N_{\text{EX-BC}}$ ) as follows:

删除了: external

245 
$$n_{\text{EX-BC}}(\log D_p) = N_{\text{EX-BC}} \times n(\log D_p) \quad (4)$$
  
246 where  $n(\log D_p)$  is the function of the aerosol number size distribution,  $D_p$  is the  
247 mobility diameter.

删除了: (3)

248 By assuming that the particles are spherical (Rader and McMurry, 1986), the mass  
249 size distribution of Ex-BC ( $M_{\text{EX-BC}}$ ) was obtained as follows:

250 
$$M_{\text{EX-BC}}(\log D_p) = \frac{\pi}{6} D_p^3 \rho n_{\text{EX-BC}}(\log D_p) \quad (5)$$

删除了: (4)

251 where  $D_p$  is the mobility diameter,  $\rho$  is the effective density of Ex-BC, and  $n_{\text{EX-BC}}(\log$   
252  $D_p)$  is the function of the number size distribution of Ex-BC, respectively. By reviewing

删除了: Here

253 and summarizing the existing results about, we show that typical values of density for

删除了: assume

254 the freshly emitted or externally mixed BC observed in the winter of urban Beijing or

删除了: the Ex-BC effective

255 North China Plain spans over 0.14-0.50 g cm<sup>-3</sup>, with mean of ~0.40±0.10 g cm<sup>-3</sup> (Fig.

删除了: is 0.40 g cm<sup>-3</sup> according to previous measurements reported...

256 S3), in the size range of 100 to 300 nm, where the mass concentration of externally

删除了: (

257 mixed BC accounted for a large proportion in urban Beijing (Geller et al., 2006; Peng

258 et al., 2016, 2017; Wu et al., 2019; Liu et al., 2020; Zhao et al., 2022). Therefore, an

删除了: ).

259 average  $\rho_{\text{EX-BC}}$  of 0.4 g cm<sup>-3</sup> was used for calculating the mass concentration of

The Ex-BC mass size distributions

260 externally-mixed BC in our study. The uncertainty analysis exhibits that the variations

删除了: modelled as a single

274 of the  $\rho_{\text{Ex-BC}}$  could lead to an average deviation of  $\pm 10\%$  in the calculating In-BC  
275 density (Fig. 3e) by increasing the  $\rho_{\text{Ex-BC}}$  from 0.1 to 0.6 g cm<sup>-3</sup>, showing a small impact  
276 on the retrieved result. Uncertainty analyses due to the variations of  $\rho_{\text{Ex-BC}}$  were given  
277 in section 2.3.

278 The mass size distribution of Ex-BC was fit using the log-normal distribution as  
279 shown in Fig. S4 (Wu et al., 2017; Liu et al., 2019a; Zhao et al., 2022). Thus, the bulk  
280 mass concentration of Ex-BC can be calculated from the integration of the mass size  
281 distribution:

$$282 \quad m_{\text{Ex-BC}} = \int_{D_{\text{start}}}^{D_{\text{end}}} M_{\text{Ex-BC}}(\log D_p) d \log(D_p) \quad (6)$$

$$283 \quad m_{\text{In-BC}} = m_{\text{BC}} - m_{\text{Ex-BC}} \quad (7)$$

284 where  $D_{\text{start}}$  and  $D_{\text{end}}$  are the lower and upper size limit,  $M_{\text{Ex-BC}}(\log D_p)$  is the function  
285 of the Ex-BC mass size distribution. We then obtained the bulk mass concentration of  
286 internally mixed BC ( $m_{\text{In-BC}}$ ) by subtracting  $m_{\text{Ex-BC}}$  from the bulk BC mass  
287 concentration measured by AE33 in equation 7.

### 288 2.2.2 Retrieving the density of BC

289 For retrieval of the density of BC, the principal idea is to use the measured  $\kappa_{\text{gf}}$  to  
290 calculate the density of BC based on the Zdanovskii–Stokes–Robinson (ZSR) mixing  
291 rule (Stokes and Robinson, 1966; Zdanovskii, 1948) with the chemical composition  
292 measured by AMS (Petters & Kreidenweis, 2007). In the retrieval, several aspects are  
293 concerned. First, since the ZSR rule is to assume the aerosol particles are internally  
294 mixed, the  $\kappa_{\text{gf}}$  value of the more MH mode ( $\kappa_{\text{gf-MH}}$ ) is thus applied for retrieving the

删除了: S2

删除了: D.

删除了: 2019

删除了: 5

删除了: 6

删除了: minus

删除了: the

删除了: 6

删除了: ACSM

删除了: with an assumption of

305 density of internally mixed BC. Second, since the size distribution of BC number  
 306 concentration is usually with peaks between 100 and 200 nm (Liu et al., 2019a; Yu et  
 307 al., 2020; Zhao et al., 2022), the  $\kappa_{gf-MH}$  value of particles in accumulation mode was  
 308 averaged and applied for the retrieval. Previous studies showed an independence of  $\kappa_{gf-}$   
 309 MH on particle size when the  $D_p > 100$  nm during the campaign period (Fan et al., 2020).  
 310 Therefore, the average of  $\kappa_{gf-MH}$  in accumulation mode is reasonable for the  
 311 determination of the In-BC density. In addition, because the inversion including  
 312 measurements from HTDMA and HR-AMS, a total mass closure of the measured  
 313 aerosol particles was conducted between the two techniques by comparing the mass  
 314 concentration of  $PM_{10}$  and the results are well consistent (Fig. S5). The density of  
 315 internally mixed BC (In-BC),  $\rho_{In-BC}$  is then derived from the following equations:

$$316 \quad \kappa_{gf-MH} = \kappa_{chem} = \sum_i \varepsilon_i \kappa_i = \frac{v_{inorg}}{v_{total}} \kappa_{inorg} + \frac{v_{SOA}}{v_{total}} \kappa_{SOA} + \frac{v_{In-POA}}{v_{total}} \kappa_{POA} + \frac{v_{In-BC}}{v_{total}} \kappa_{BC} \quad (8)$$

317 where  $\kappa_{gf-MH}$  is the hygroscopic parameter of the more hygroscopic (MH) mode,  $\kappa_{chem}$   
 318 is the hygroscopic parameter of aerosol particles in the mixed composition and can be  
 319 calculated based on chemical volume fractions using a simple rule (Stokes and  
 320 Robinson, 1966; Petters & Kreidenweis, 2007),  $\kappa_i$  is the hygroscopic parameter of each  
 321 pure composition and  $\varepsilon_i$  is the volume fraction of the individual components in the  
 322 internal-mixed particle.  $v_{inorg}$ ,  $v_{SOA}$  and  $v_{In-POA}$  are the volume of the inorganic, SOA  
 323 and internally mixed POA species, and can be calculated as follows:  $v_{inorg} = \frac{m_{inorg}}{\rho_{inorg}}$ ,  
 324  $v_{SOA} = \frac{m_{SOA}}{\rho_{SOA}}$ , and  $v_{In-POA} = \frac{m_{In-POA}}{\rho_{POA}}$ .  $v_{total}$  is the total volume of all the species and can be

325 written as  $v_{total} = \frac{m_{inorg}}{\rho_{inorg}} + \frac{m_{SOA}}{\rho_{SOA}} + \frac{m_{In-POA}}{\rho_{POA}} + \frac{m_{In-BC}}{\rho_{In-BC}}$ . In equation (8),  $\kappa_{BC}$  and  $\kappa_{POA}$  are  
 326 assumed to be 0. Then, the  $\rho_{In-BC}$  can be calculated based on its mass concentration and

删除了: -

删除了: D.

删除了: 2019

删除了: , which

删除了: ), was averaged and applied for the retrieval.

删除了: ACSM

删除了: S3

删除了: -

删除了: 7

删除了: by

删除了: the

删除了: 7

339 volume as follows:

340 
$$\rho_{In-BC} = \frac{m_{In-BC}}{\left( \frac{m_{inorg}}{\rho_{inorg}} + \frac{m_{SOA}}{\rho_{SOA}} \right) \frac{\kappa_{inorg}}{\kappa_{gf-MH}} + \frac{m_{inorg}}{\rho_{inorg}} \frac{m_{SOA}}{\rho_{SOA}} \frac{m_{In-POA}}{\rho_{POA}}} \quad (9)$$

341 where,  $m_{In-BC}$  is the mass concentration of internally mixed BC,  $m_{inorg}$  and  $m_{SOA}$  are the  
342 mass concentrations of the inorganic species and SOA, which are measured by the AMS.

343  $m_{In-POA}$  is the mass concentrations of internally mixed POA and can be calculated  
344 subtracting the mass fraction of NH-POA from the total mass concentrations of POA.

345  $\rho_{inorg}$ ,  $\rho_{SOA}$  and  $\rho_{POA}$  are the density of the inorganic species, SOA and POA. Since the  
346 AMS measures the concentrations of the organic and inorganic ions, including  $SO_4^{2-}$ ,

347  $NO_3^-$ ,  $NH_4^+$ ,  $Cl^-$ . Here inorganic species were derived by applying a simplified ion  
348 pairing scheme (Gysel et al., 2007) to convert mass concentrations of ions to the

349 inorganic salts as follows:

351 
$$n_{NH_4NO_3} = n_{NO_3^-}$$
  
352 
$$n_{NH_4HSO_4} = \min(2n_{SO_4^{2-}} - n_{NH_4^+} + n_{NO_3^-}, n_{NH_4^+} - n_{NO_3^-})$$
  
353 
$$n_{(NH_4)_2SO_4} = \max(n_{NH_4^+} - n_{NO_3^-} - n_{SO_4^{2-}}, 0)$$
  
354 
$$n_{H_2SO_4} = \max(0, n_{SO_4^{2-}} - n_{NH_4^+} + n_{NO_3^-}) \quad (10)$$

354 where  $n$  represents the number of moles, then the mass concentrations were obtained  
355 by the number of moles times the molar mass of each inorganic salts. Because the  
356 maximum value of the  $n_{H_2SO_4}$  was zero in this campaign. Three inorganic salts

357 including  $NH_4HSO_4$ ,  $(NH_4)_2SO_4$ , and  $NH_4NO_3$  were applied in our study. The densities  
358 for inorganic salts were taken from previous studies (Gysel et al., 2007; Wu et al., 2016).

359 Here the densities for three inorganics are 1.78, 1.77 and 1.72  $g\ cm^{-3}$ , respectively. By  
360 summarizing the previous studies (Gysel et al., 2007; Dinar et al., 2006), 1.4  $g\ cm^{-3}$  was

删除了: 8

删除了: internal-

删除了: ACSM

删除了: internal-

删除了: by using

删除了: minus the mass fraction of NH-POA.

删除了: 2007).

删除了: and organics

删除了: referred

删除了: the articles published

删除了: 79

删除了: And

373 selected as the density of SOA ( $\rho_{SOA}$ ). The density of POA ( $\rho_{POA}$ ) is assumed to be 1.0  
 374 g cm<sup>-3</sup> for urban environments, which is similar to the lubricating oil (Wu et al., 2016).  
 375 Considering the cooking organic aerosols represent a high contribution to POA in urban  
 376 environments, a density of 0.85 g cm<sup>-3</sup> chosen as the mean density for the rapeseed oil  
 377 and oleic acid (Reyes-Villegas et al., 2018) was also used to evaluated the result as  
 378 shown in section 2.3. The values of  $\kappa$  for inorganic components are 0.56 for NH<sub>4</sub>HSO<sub>4</sub>,  
 379 0.48 for (NH<sub>4</sub>)<sub>2</sub>SO<sub>4</sub> and 0.58 for NH<sub>4</sub>NO<sub>3</sub>, along with the best-fit values for the three  
 380 inorganic salts (Petters & Kreidenweis, 2007 and Gunthe et al., 2009). The  $\kappa_{SOA}$  is  
 381 assumed to be 0.15 according to the field studies in urban areas (Chang et al., 2010;  
 382 Kawana et al., 2016).

删除了: and

删除了: are

删除了: as 1.4 and

删除了: .

删除了: each pure component was refereed from Petters & Kreidenweis, 2007 and Gunthe et al., 2009. For the

删除了: compounds, the  $\kappa$  values

删除了: .

383 Note that, this method fails to retrieve the BC density when organics account for  
 384 a large fraction (>60 %). This is because that a higher fraction of OA usually  
 385 corresponds to lower total volume of all the species (Fig. S6), yielding negative values  
 386 for  $v_{In-BC}$  introduced in equation 11. As a result, 61% of the data observed during the  
 387 campaign were valid for calculating the BC density.

移动了(插入) [1]

移动了(插入) [2]

$$388 \quad v_{In-BC} = \frac{v_{inorg}\kappa_{inorg} + v_{SOA}\kappa_{SOA}}{\kappa_{gf-MH}} - v_{inorg} - v_{SOA} - v_{In-POA} \quad (11)$$

389 Similarly, the bulk density of BC ( $\rho_{bulk-BC}$ ) is calculated with the same method as  
 390 that for calculating the  $\rho_{In-BC}$ . When calculating the  $\rho_{bulk-BC}$ , the bulk  $\kappa_{gf}$  value measured  
 391 by HTDMA is applied with the assumption of all the aerosol particles are internally  
 392 mixed.

移动了(插入) [3]

401 **2.3 Uncertainties and limitations**

402 For the retrieval, the assumptions on the values of  $\kappa_{\text{SOA}}$ ,  $\rho_{\text{POA}}$ ,  $\rho_{\text{SOA}}$  and  $\rho_{\text{Ex-BC}}$  as  
403 well as the fraction of primary organic aerosols in non-hygroscopic or hygroscopic  
404 mode would add uncertainty in the inferred values of ambient internally mixed BC  
405 density. For example, the freshly emitted POA particles might consistently be coated  
406 with the secondary particles during the aging process, resulting in changes of the  $N_{\text{NH-POA}}$   
407  $\rho_{\text{POA}}$ . However, a real-time variation of the  $N_{\text{NH-POA}}$  is not yet available due to the lack  
408 of such measurements data. Applying the rough fractions of hydrophobic POA only  
409 under three different atmospheric conditions could still cause uncertainties. Also, the  
410 densities of POA and SOA may differ due to their precursors, emission sources and the  
411 formation mechanisms in ambient atmosphere (Alfarra et al., 2006; Reyes-Villegas et  
412 al., 2018). And the density of Ex-BC is generally characterized by the morphology and  
413 size (Wu et al., 2019). In addition, the value of  $\kappa_{\text{SOA}}$  spans largely due to the variability  
414 in the emissions of gas precursors and formation processes under different atmospheric  
415 conditions (Zhang et al., 2015; Liu et al., 2021b). Therefore, we examined the  
416 sensitivities of In-BC density to the variations of these factors, as exhibited in Fig. 1  
417 and Fig.2.

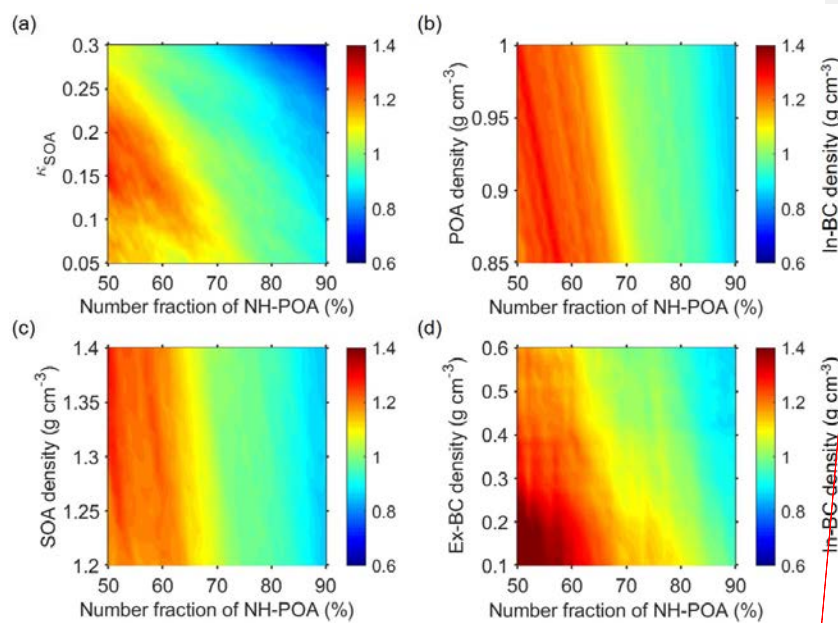
418 The figures show that the In-BC density gradually decreases with the increment of  
419 the  $N_{\text{NH-POA}}$ , implying the higher fraction of bare POA particles correspond to the early  
420 aging stage of aerosol particles. With increase of  $\kappa_{\text{SOA}}$ , the In-BC density is generally  
421 reduced, but with small fluctuations (Fig.1a, Fig. 2b). This suggests a complex impact  
422 of assumptions of  $\kappa_{\text{SOA}}$  on the retrieved BC density. In addition, the In-BC density

删除了: -mixed BC density.

删除了: 1. Within a typical atmospheric observed range of 50-90 % for the  $N_{\text{NH-POA}}$  (Liu et al., 2021), the assumption on  $N_{\text{NH-POA}}$  can lead to relative deviations (uncertainty) of -20 %~+30 % for the retrieved BC density (Fig. 2a).

移动了(插入) [4]

428 decreases very slightly as  $\rho_{\text{Ex-BC}}$  increases (Fig. 2e), suggesting applying a larger  $\rho_{\text{Ex-BC}}$   
429 would derive smaller values for In-BC density. The In-BC density is insensitive to the  
430 changes of the density of POA and SOA, showing an almost negligible effect on the  
431 retrieved results (Fig. 2c and d).



移动了(插入) [5]

432  
433 **Figure 1.** Sensitivities of In-BC density to the variations in the number fraction of  
434 nearly hydrophobic (NH) POA and hygroscopic parameter of OA ( $k_{\text{SOA}}$ ) (a), POA  
435 density (b), SOA density (c) and the externally mixed BC density (d).

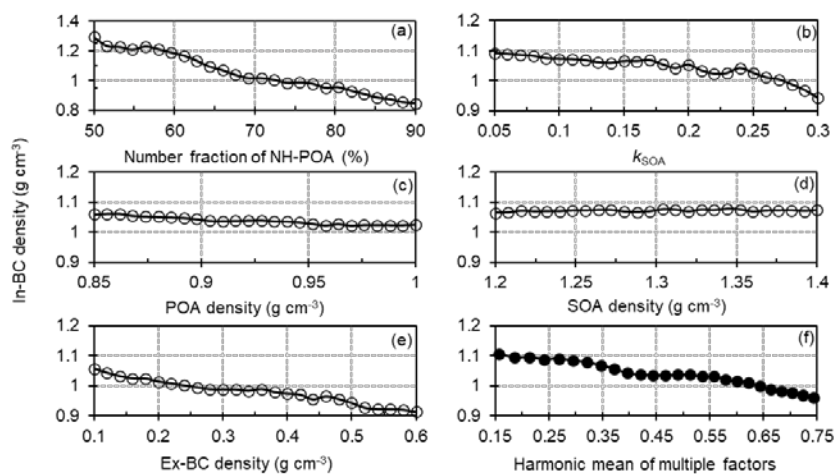
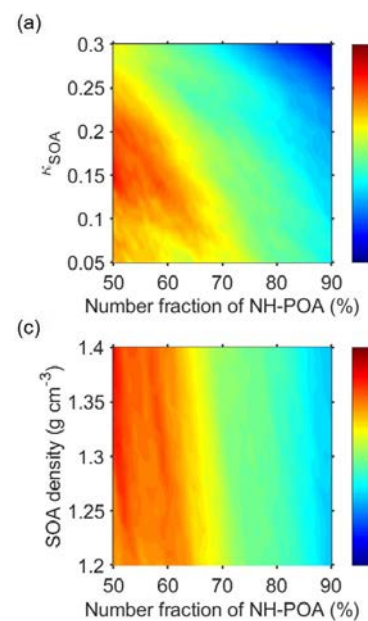


**Figure 2.** Sensitivity of the In-BC density to variations in the number fraction of nearly hydrophobic (NH) POA (a), the hygroscopic parameter of SOA (b), the POA density (c), the SOA density (d), the externally mixed BC density (e) and the harmonic mean of multiple factors (f).

The uncertainty analysis shows that, by comparing the results based on the mean fractions of the  $NF_{NH-POA}$  with a typical atmospheric observed range of 50-90 % for the  $NF_{NH-POA}$  (Liu et al., 2021a), we show that the assumption on  $NF_{NH-POA}$  can lead to relative deviations (uncertainty) of -17 % - +27 % for the retrieved BC density (Fig.3a).

In addition, unlike inorganics (eg.,  $NH_4HSO_4$ ,  $(NH_4)_2SO_4$  and  $NH_4NO_3$ ), which the hygroscopicity has been already well-understood (Petters and Kreidenweis, 2007), the hygroscopicity of organic species varies largely due to the complexity in organic aerosol constituents. Therefore, the assumption of the values of  $\kappa_{SOA}$  will add the uncertainty in the calculation of BC density. Previous studies have suggested that the organics has a wide range of  $\kappa$  values ranging from 0.05 to 0.3 (Jimenez et al., 2009;

删除了:.



上移了 [5]:

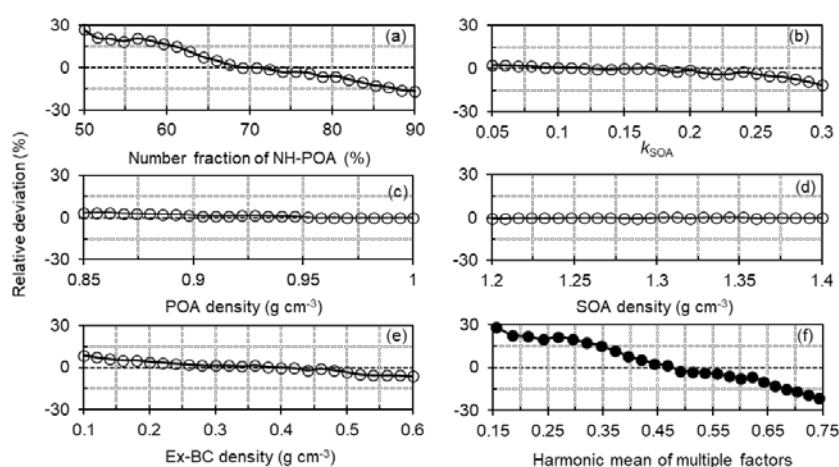
**Figure 1.** Sensitivities of In-BC density to the variations in the number fraction of nearly hydrophobic (NH) POA and hygroscopic parameter of OA ( $\kappa_{SOA}$ ) (a), POA density (b), SOA density (c) and the externally

删除了: -mixed BC density (d).



458 Mei et al., 2013). Thus, the sensitivity test has also been done to examine the effect due  
 459 to changes in  $\kappa_{\text{SOA}}$  on calculating the density of BC (Fig. 1a). The result shows that the  
 460 assumption of  $\kappa_{\text{SOA}}$  value can cause an average relative deviation of -10 % - +3 % in  
 461 calculating the density of In-BC (Fig. 3b).

删除了: 20 %-+



462  
 463 **Figure 3.** Relative deviations of the number fraction of nearly hydrophobic (NH) POA  
 464 to the In-BC density (a), the hygroscopic parameter of OA to the In-BC density (b), the  
 465 POA density to the In-BC density (c), the SOA density to the In-BC density (d), the  
 466 externally-mixed BC density to In-BC density (e) and the combined deviations based  
 467 on multiple factors mentioned above (f).

468 However, the sensitivity test shows that the impact of both the  $\rho_{\text{POA}}$  and  $\rho_{\text{SOA}}$   
 469 variations on the BC density estimation is very small or even negligible (Fig. 1b, c). By  
 470 varying the  $\rho_{\text{POA}}$  from 0.85 to 1.0 g cm<sup>-3</sup> and the  $\rho_{\text{SOA}}$  from 1.2 to 1.4 g cm<sup>-3</sup> according  
 471 to the literatures (Noureddini et al., 1992; Alfara et al., 2006; Reyes-Villegas et al.,  
 472 2018), the retrieval uncertainties in the BC density are within  $\pm 5$  % and  $\pm 1$  %

上移了 [4]: 2b).

删除了: 10

删除了: 5 % <object>

477 respectively (Fig. 3c, d). For  $\rho_{\text{Ex-BC}}$ , it exhibits that the evolution of the  $\rho_{\text{Ex-BC}}$  could lead  
 478 to an average deviation of  $\pm 10\%$  in calculating In-BC density (Fig. 3e) when  
 479 increasing the values of  $\rho_{\text{Ex-BC}}$  from 0.1 to 0.6  $\text{g cm}^{-3}$ , which represents a typical range  
 480 in ambient atmosphere (Wu et al., 2019; Liu et al., 2020). A combined uncertainty ( $\delta$ )  
 481 caused by the multiple factors ( $\delta_i$ ), which is calculated by equation 12, is  $-21\%$ – $+29\%$   
 482 as shown in Fig. 3f.

$$\delta = \sqrt{\sum_{i=1}^n \delta_i^2} \quad (12)$$

### 484 3 Results and Discussion

#### 485 3.1 Retrieved mixing state and density of BC: comparison and validation

486 Figure 4a shows retrieved time series of the mixing state of ambient BC during the  
 487 campaign. Large temporal variations of the mass fraction of internally and externally  
 488 mixed BC are presented during the observed period at the sites. The temporal changes  
 489 should be related to the atmospheric aging process or diurnal variations of emissions  
 490 (Liu et al., 2019a; Fan et al., 2020). Statistically, the average mass fraction of externally  
 491 and internally mixed BC is  $20 \pm 18\%$  and  $80 \pm 20\%$  respectively, showing that most of  
 492 the BC particles were aged and internally mixed with other components. Previous  
 493 studies at urban sites have shown that the co-existence of the externally mixed BC in  
 494 the ambient atmosphere (Schwarz et al., 2008; Cheng et al., 2012; Chen et al., 2020)  
 495 due to continuous combustion processes (e.g., vehicle exhaust and residential sector)  
 496 (Wang et al., 2017; Liu et al., 2019a). Our results are basically comparable with those

删除了: 2c...c, d). Similarly...or  $\rho_{\text{Ex-BC}}$ , it exhibits that the variations...evolution of the  $\rho_{\text{Ex-BC}}$  would **Figure 2**. Relative deviations of the number fraction of nearly hydrophobic (NH) POA...ould lead to the In-BC density (a), the hygroscopic parameter of OA to the In-BC density (b), the POA density to the In-BC density (c), the SOA density to the In-BC density (d), the externally-mixed BC density to In-BC density (e) and the combined deviations based on multiple factors mentioned above (f).  
cause

删除了: (...n calculating In-BC density (Fig. 2e) in retrieved In-BC density...e) when increasing the values of  $\rho_{\text{Ex-BC}}$  from 0.10... to 0.60...  $\text{g cm}^{-3}$ , which represents a typical range of  $\rho_{\text{Ex-BC}}$ ...in ambient atmosphere (Wu et al., 2019; Liu et al., 2020). A combined uncertainty ( $\delta$ ) caused by the multiple factors ( $\delta_i$ ), which is calculated by the ...quation 9...2, is  $-23\%$ – $+31\%$ ... $-29\%$  as shown in Fig. 2f

删除了: (9)

上移了 [1]: Note that, this method fails to retrieve the BC density when organics account for a large fraction ( $>60\%$ ). This is because that a higher fraction of OA usually corresponds to lower total volume of all the species (Fig.

上移了 [2]: % of the data observed during the campaign were valid for calculating the BC density.

$$v_{\text{In-BC}} = \frac{v_{\text{inorg}}\kappa_{\text{inorg}} + v_{\text{SOA}}\kappa_{\text{SOA}}}{\kappa_{\text{gf-MH}}} - v_{\text{inorg}} - v_{\text{SOA}}$$

上移了 [3]: When calculating the  $\rho_{\text{bulk-BC}}$ , the bulk  $\kappa_{\text{gf}}$  value measured by HTDMA is applied with the assumption of all the aerosol particles are internally mixed.

删除了: S4), yielding negative values for  $v_{\text{In-BC}}$  introduced in equation 10. As a result, 62

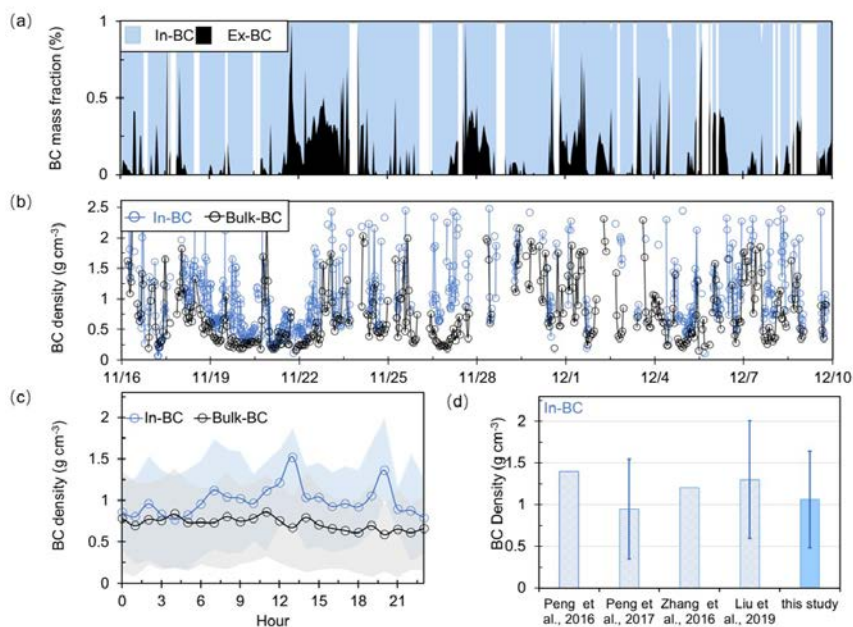
删除了: 10)

Similarly, the bulk density of BC ( $\rho_{\text{bulk-BC}}$ ) is calculated with the same method as that for calculation the  $\rho_{\text{In-BC}}$ .

删除了: 3a...a shows retrieved time series of the mixing state of ambient BC during the campaign. Large temporal variations of the mass fraction of internal...nternally and

下移了 [6]: directly measured or indirectly retrieved previously reported results. For example, Chen et al.,

删除了: 2020 found that the mass fraction of internal mixed BC particles was nearly to be



618

619 **Figure 4.** (a) Time series of the mass fraction of the retrieved internal- and external-  
 620 mixed BC; (b) Time series of the retrieved density of the bulk and internal- mixed BC  
 621 (In-BC); (c) Diurnal variation of the retrieved density of bulk and In-BC; (d)  
 622 Comparison of the results of the derived In-BC density in this study with that reported  
 623 in literatures.

624 directly measured or indirectly retrieved previously reported results. For example, Chen  
 625 et al., 2020 found that the mass fraction of internally mixed BC particles was nearly to  
 626 be ~80–90 % in summer of Beijing based on VTDMA measurements. Liu et al. (2020),  
 627 using a tandem system with an aerodynamic aerosol classifier and SP2, reported that  
 628 the mass fraction of internally BC-containing particles would increase with increasing  
 629 size and reach ~70 % in Beijing. Overall, the mass fraction obtained in our study is  
 630 comparable with those reported in urban Beijing. Previous studies also displayed that

删除了: 3

移动了(插入) [6]

删除了: .,

删除了: internal

634 the significant diversity of the BC mixing state among emission conditions and coating  
635 process (Shiraiwa et al., 2008; Pan et al., 2017; Zhang et al., 2020b). Accordingly, the  
636 densities of the bulk and internally mixed BC present apparent fluctuations as shown in  
637 Fig. 4b, which is significantly affected by the variations of BC emission sources and its  
638 rapid aging process. The density of the In-BC during daytime was generally higher than  
639 that at night (Fig. 4c). The elevated BC density during daytime is likely due to that the  
640 strong photochemical processes promote the aging of BC particles, which resulted in a  
641 conversion from uncompact structure to compact and regular spherical shapes of BC  
642 (Qiao et al., 2018; Liu et al., 2019b; Zhou et al., 2022). The lift in BC density around  
643 20:00 LT might indicate that the BC particles would be rapidly coated with the SIA  
644 particles and continuously aged in the polluted period due to the heterogeneous  
645 reactions of SIA in urban regions (Zhang et al., 2016; Peng et al., 2017). Actually,  
646 following the haze evolution, the fraction of nearly hydrophobic group reduced rapidly  
647 (Fig. S7). Consequently, the average density of In-BC increased obviously from the  
648 clean conditions to the polluted periods (Fig. S8). A slight decrease was observed in the  
649 bulk BC density during traffic hours. This is likely associated with the continues  
650 emissions (e.g., vehicle exhaust) that lead to uncoated or uncompact BC particles in  
651 this period. The diurnal cycle in In-BC density is consistent with the coating thickness  
652 measured by a tandem CPMA-SP2-DMA-SP2 (Liu et al., 2020), demonstrating that the  
653 new method can derive the density of ambient BC particles reasonably. Averagely, the  
654 bulk and internally mixed BC densities are with campaign averaged values of 0.7±0.5  
655 and 1.1±0.6 g cm<sup>-3</sup> respectively, which are much less than 1.8 g cm<sup>-3</sup>, implying that the

删除了: 2020

删除了: internal

删除了: 3b

删除了: were

删除了: 3c

删除了: 2018; H. Liu et al., 2019; Zhou et al., 2022). The slightly decreases were observed both in the bulk BC and In-

删除了: more

删除了: urban regions.

删除了: cycles

删除了: are

删除了: that

删除了: internal-

删除了: 73

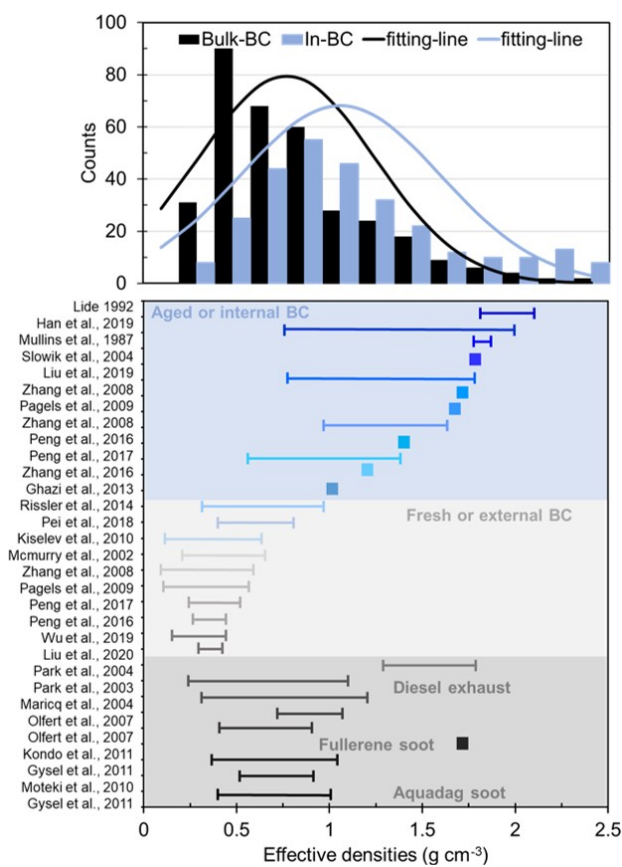
删除了: 46

删除了: 11

删除了: 54

673 BC particles is not a void-free spheres in the urban atmosphere. The results of In-BC  
 674 density are comparable with that observed at the other sites in North China Plain (NCP)  
 675 as shown in Fig. 4d, illustrating that the BC effective density retrieved by this method  
 676 is within the range of field measurements.

删除了: 3d



677  
 678 **Figure 5.** The probability distribution function (PDF) of the retrieved density of bulk  
 679 and In-BC and the measured density distribution spectrum of BC from different sources  
 680 reported in literatures.

681 Based on both field measurements (e.g. Lide 1992; Zhang et al., 2016; Wu et al.,  
 682 2019; Liu et al., 2019b) and laboratory studies (e.g. McMurry et al., 2002; Park et al.,

删除了: H.

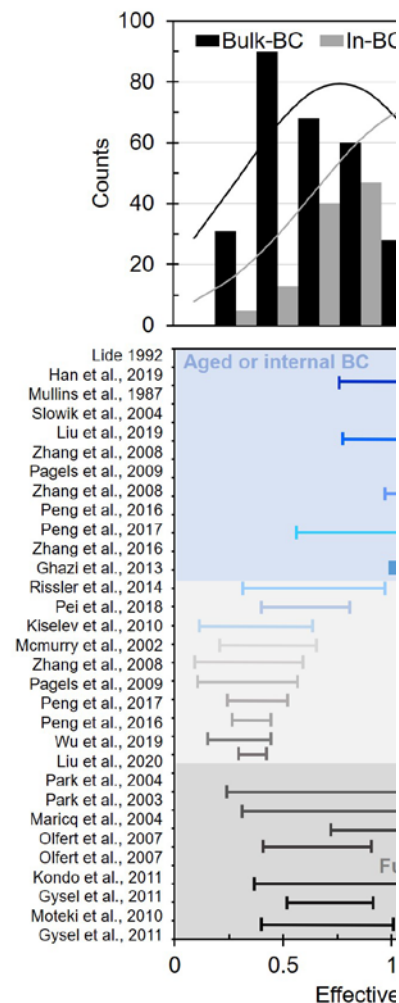
删除了: 2019

删除了: McMurry

2003, 2004; Olfert et al., 2007; Kiselev et al., 2010; Gysel et al., 2011, 2012), the BC density from diverse combustion sources or representing different aging degree has been obtained and ranges widely from 0.14 to 2.1 g cm<sup>-3</sup>, as has been summarized and shown in Fig. 5. Mean probability distribution function (PDF) of the density of bulk and In-BC retrieved by this study is also presented in Fig. 5. It shows that the retrieved density of bulk BC exhibits a dominant mode with a peak value of 0.7 g cm<sup>-3</sup>, which is situated between the typical density range of those externally mixed and internally mixed BC measured previously. For the In-BC, the PDF is with a peak value at 1.1 g cm<sup>-3</sup>, but ranges widely from ~0.5 to 2.5 g cm<sup>-3</sup>, which indicates various morphologies, different aging degree and compositions of ambient BC particles due to the complex impact of multiple local sources and aging processes during the observed period in urban Beijing. Overall, the retrieved values for In-BC fall within the range of typical internal mixed BC reported in the literatures, verifying the reliability of our inversion results.

### 3.2 Sensitivity of predicted $N_{CCN}$ to changes of BC density

A previous study showed that the use of an inaccurate density value of BC particles would result in large bias in estimating  $\kappa$  of ambient aerosol particles with the ZSR mixing rule (Fan et al., 2020), as would further lead to uncertainties in prediction of  $N_{CCN}$  and relevant climate effects. Considering the large variation range of BC density during the campaign, which is closely associated with its morphology or degree of its aging, we further examine the sensitivity of critical supersaturation ( $S_c$ ), critical



删除了:

Figure 4. The probability distribution function (PDF) of the retrieved density of bulk and In-BC and the measured density distribution spectrum of BC from different sources reported in literatures.

删除了: It has been studied

删除了: an inappropriate ...he use of the ...n inaccurate density value of BC particles will



734 diameter ( $D_{cut}$ ) and predicted  $N_{CCN}$  to variations of BC density (Fig. 6). Here, we use  
 735 the critical diameter and particle number size distribution to calculate  $N_{CCN}$ . The method  
 736 to derive the critical diameter is based on Köhler theory and ZSR rule.

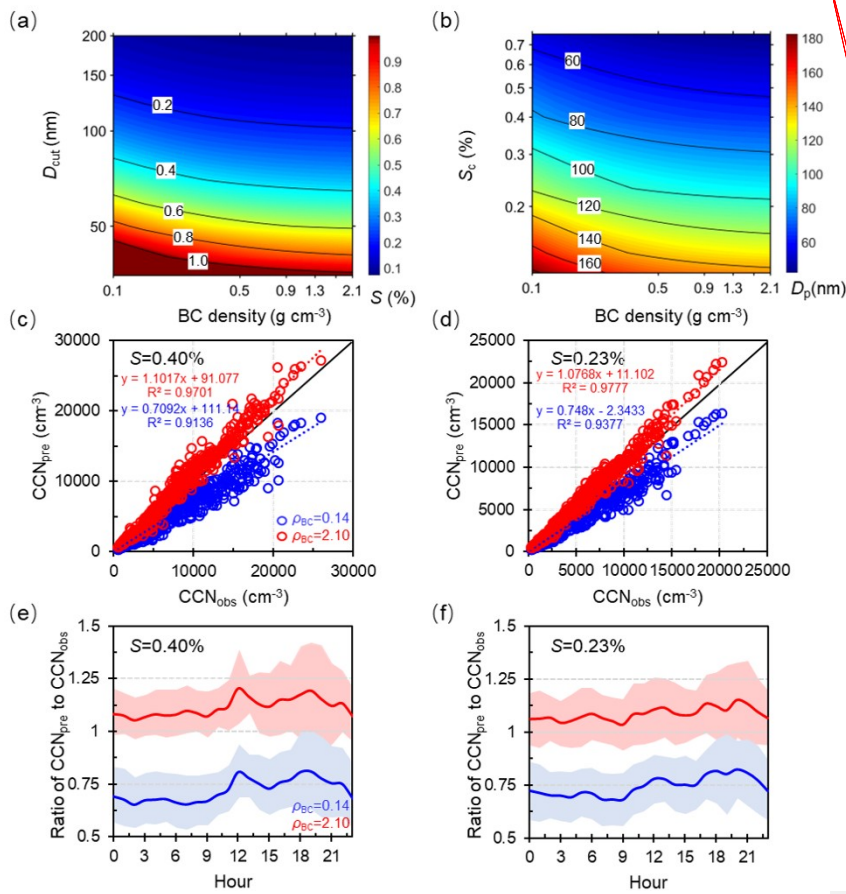
删除了: 5

下移了 [7]: to derive the critical diameter is based on Köhler theory and ZSR rule.

下移了 [8]: to evaluate the effect of BC density and mixing state on prediction of CCN number concentrations. The detailed calculation methods are presented in the supporting information (SI: Methods) or referenced from Ren et al., 2018.

删除了: Three closure studies were used

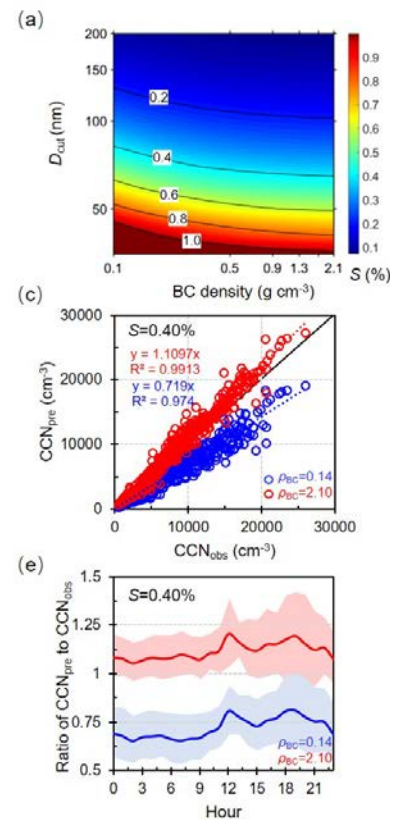
移动了(插入) [7]



737  
 738 **Figure 6.** Sensitivity of critical supersaturation ( $S_c$ ) (a) and diameter ( $D_{cut}$ ) (b) to the  
 739 variations in BC density; Predicted  $N_{CCN}$  as a function of measured  $N_{CCN}$  by varying the  
 740 density from 0.14 to 2.1  $g\ cm^{-3}$  at  $S=0.40\%$  (c) and  $S=0.23\%$  (d), the black solid line  
 741 is the 1:1 line; Diurnal variations in the ratio of predicted-to-measured  $N_{CCN}$  at  $S=0.40\%$   
 742 (e) and  $S=0.23\%$  (f).

删除了:

删除了: 5



754 The results show that, by varying the value of density from 0.14 to 2.1 g cm<sup>-3</sup> that  
755 represents the lower and upper limit of BC density in the atmosphere, the  $D_{cut}$  reduces  
756 apparently at a given supersaturation ( $S$ ) (Fig. 6a), or similarly, the  $S_c$  decreases rapidly  
757 for a given particle size (Fig. 6b). The results show that the changes of the  $D_{cut}$  and  $S_c$   
758 are more sensitive when the BC density is below 1.0 g cm<sup>-3</sup>. And the effects on the  $D_{cut}$   
759 and  $S_c$  both gradually weakened with the increase of BC density. This shows that it is  
760 critical to apply more accurate BC density for the aerosol particles with low aging  
761 degree in predicting CCN and its climate effect. Accordingly, the ratios of predicted-  
762 to-measured  $N_{CCN}$  ranged from 0.72 to 1.11 by varying the BC density from 0.14 to 2.1  
763 g cm<sup>-3</sup> at the typical  $S$  of 0.23 % and 0.40 % (Fig. 6c, 6d), showing an estimation  
764 uncertainty of -28 %–11 % in  $N_{CCN}$  prediction.

765 The diurnal variations in the ratio of predicted-to-measured  $N_{CCN}$  at  $S=0.40$  % and  
766 0.23 % are shown to examine the response of the BC density on  $N_{CCN}$  prediction at  
767 different time periods (Fig. 6e, 6f). By applying the lower limit of density value of 0.14  
768 g cm<sup>-3</sup>, the prediction is much worse compared to the use of the density of 2.1 g cm<sup>-3</sup> at  
769 nighttime (00:00-06:00 LT), when the latter is much closer to the real density of ambient  
770 BC (Fig. 4c). The prediction is improved substantially by applying the value of 0.14 g  
771 cm<sup>-3</sup> during evening rush hours (18:00-20:00 LT), during which the ambient BC  
772 particles is disturbed by the traffic emissions (Fig. 4c). And now, the prediction becomes  
773 worse by applying the value of 2.1 g cm<sup>-3</sup>, and an obvious overestimation by up to ~40 %  
774 is shown. The results further illustrate that it is critical to account for the real-time  
775 mixing state and density of BC particles in  $N_{CCN}$  prediction, particularly in those regions

删除了: ),

删除了: 5a

删除了: 5b

删除了: 2

删除了: 4

删除了: 5c, 5d

删除了: 5e, 5f

删除了: 3c

删除了: more externally-mixed with smaller densities

删除了: 3c

删除了: in particular



787 with heavy traffic and residential coal emissions.

788 It should be noted that the assumption of the surface tension of water would  
789 overestimate the critical diameter and underpredict CCN number concentration. While  
790 the surface tension depression might be more obvious for the small size particles (<60  
791 nm), as the fraction of organics are higher at small particles size (Meng et al., 2014; Cai  
792 et al., 2018). Here, in this study, we calculated the critical diameters at supersaturations  
793 of 0.40 % and 0.23 %, typical values in cloud, corresponding to larger sizes (> 70 nm  
794 and 90 nm) of aerosols. Therefore, the uncertainties from the application of the surface  
795 tension of pure water should be negligible (< 10 %). Here, three schemes were assumed,  
796 to evaluate the effect of BC density and mixing state on prediction of CCN number  
797 concentrations. The detailed calculation methods are presented in the supporting  
798 information (SI: Methods) or referenced from Ren et al., 2018.

移动了(插入) [8]

### 799 3.3 Using the real-time variations of BC density and mixing state to predict $N_{CCN}$

800 Figure 7 exhibits the comparisons between predicted and measured  $N_{CCN}$  at  $S$  of  
801 0.23 % and 0.40 % by accounting for the retrieved real-time variations of BC density  
802 and mixing state. It shows that the  $N_{CCN}$  can be well predicted with a slope of 1.01 and  
803 1.02 at  $S$  of 0.23 % and 0.40 % respectively (Fig. 7a, 7b), only presenting a slight  
804 deviation. The slight deviation is primarily due to the fixed value of the density for the  
805 externally mixed BC caused by the retrieved method, especially during noontime and  
806 evening rush periods (Fig. 7c and 7d).

删除了: 6

删除了: 2

删除了: 4

删除了: 0.98

删除了: 0.97

删除了: 2

删除了: 4

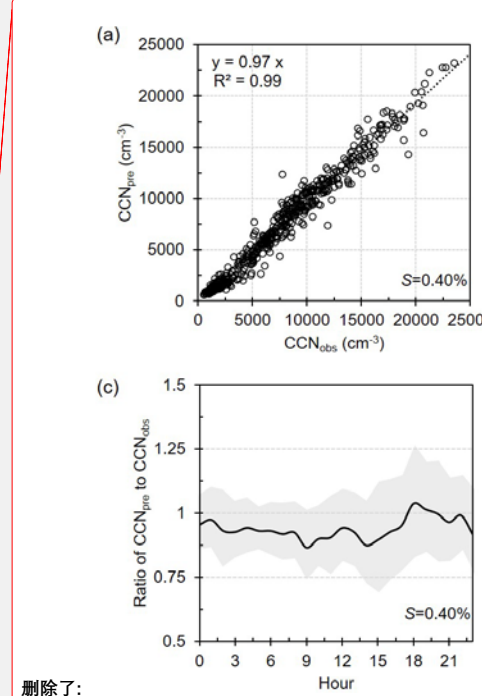
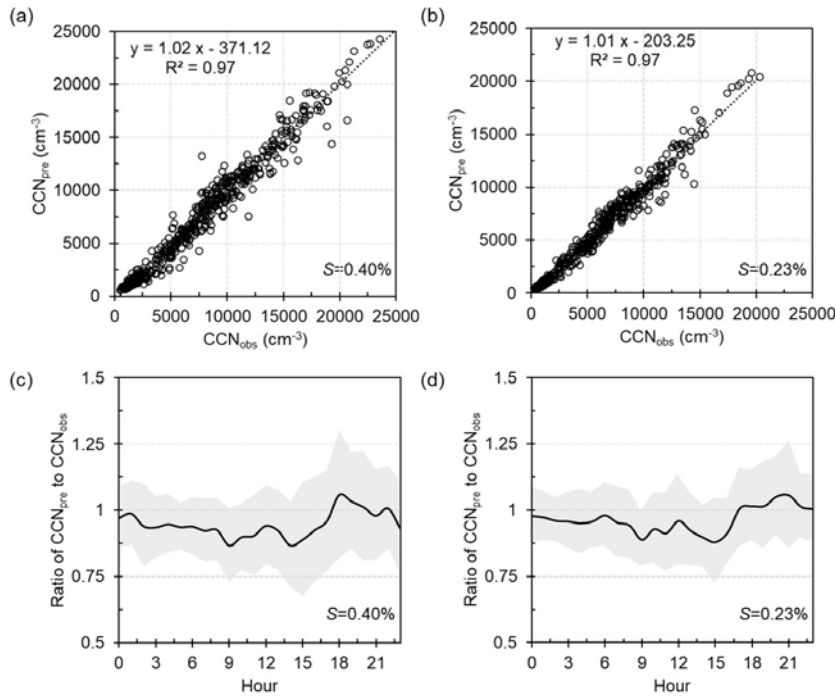
删除了: 6a, 6b

删除了: underestimation

删除了: an underestimation

删除了: 6c

删除了: 6d



819

820 **Figure 7.** Prediction CCN number concentration, using the mixing state and In-BC  
 821 density derived from HTDMAs at  $S=0.40\%$  (a) and  $S=0.23\%$  (b). Diurnal variations  
 822 in the ratio of predicted-to-measured  $N_{CCN}$  at  $S=0.40\%$  (c) and  $S=0.23\%$  (d).

823 The diurnal variations in the ratio of predicted-to-measured  $N_{CCN}$  shows the  $N_{CCN}$   
 824 can be underestimated by up to 15% at  $S=0.40\%$  during those periods. While, a slightly  
 825 overrated during the evening traffic hours and nighttime may be due to the  
 826 underestimation of the number fraction of Ex-BC. Overall, the dependence of the CCN  
 827 prediction on  $S$  is due to the size dependence of  $\kappa$  and mixing state (Zhang et al., 2017;  
 828 Liu et al., 2020; Xu et al., 2021). The better closure at  $S=0.23\%$  is because that the bulk  
 829  $\kappa$  of particles is closer to that the critical diameter corresponding to  $S=0.23\%$ , with  $D_p$   
 830 of 100-150 nm. Similarly, the effect on CCN prediction induced by the bulk mixing

删除了:

删除了: 6

删除了: by

删除了: 20

删除了: 4

删除了: 2

删除了: 2

838 state would be more critical for smaller particles, corresponding to the critical diameter  
839 at high  $S$ .

840 Overall, when considering the effective density of BC relevant to its mixing state,  
841 the CCN closure achieves. Previous studies have shown that the fresh emitted BC  
842 particles may convert from fractal-like aggregates to a compact structure and its density  
843 would increase with the aging process (Pagels et al., 2009; Rissler et al., 2014; Peng et  
844 al., 2016; Liu et al., 2019b; Zhang et al., 2020a, 2022), but the actual density of In-BC  
845 may be lower than  $1.8 \text{ g cm}^{-3}$  in the ambient atmosphere according to this study.  
846 Therefore, the currently applied value represents a density of the void-free structure of  
847 BC particles may cause an overestimation in CCN prediction.

#### 848 4 Conclusions

849 The mixing state and effective density of BC changed through heterogenous  
850 chemistry process and thus would cause uncertainty in evaluating its CCN activity. In  
851 this study, we develop a new method to retrieve the mixing state and effective density  
852 of ambient BC using field measurements and the Köhler theory. The uncertainty of the  
853 new retrieval method was evaluated within  $\pm 30\%$ , which is primarily caused to  
854 assuming the  $\kappa_{\text{SOA}}$  and the fraction of primary organic aerosols in non-hygroscopic or  
855 hygroscopic mode. The retrieved results show that most of the BC particles were aged  
856 and internally mixed with other components, with mean mass fraction of  $80 \pm 20\%$ .  
857 Averagely, the retrieved densities of the bulk and internal-mixed BC are  $0.7 \pm 0.5$  and  
858  $1.1 \pm 0.6 \text{ g cm}^{-3}$  respectively, but ranges widely from  $\sim 0.1$  to  $2.5 \text{ g cm}^{-3}$ , indicating

删除了: H.

删除了: 2019

删除了: 2020

删除了: causes

删除了: by assumptions of

删除了: -

删除了:  $79 \pm 18$

删除了:

删除了: 73

删除了: 46

删除了: 11

删除了: 54

删除了: 4

872 various morphologies, different aging degree and compositions of ambient BC particles  
873 due to the complex impact of multiple local sources and aging processes during the  
874 observed period. The retrieved results are basically comparable with the previous  
875 observations in North China Plain.

876 Further examination shows the  $N_{CCN}$  prediction is with uncertainties of -28 %–11 %

877 at the typical  $S$  of 0.23 % and 0.40 % by varying the BC density from 0.14 to 2.1 g cm<sup>-3</sup>

878 <sup>3</sup> that represents the lower and upper limit of ambient BC particles. Moreover, the

879 prediction is found more sensitive to the variability of BC density when it is <1.0 g cm<sup>-3</sup>

880 <sup>3</sup>, suggesting a great significance to account for the effect of BC density for the aerosol

881 particles with low aging degree when evaluating the climate effect. The CCN closure

882 achieves when introducing the retrieved real-time BC density relevant to its mixing

883 state. This work provides a unique way of utilizing field observations to infer ambient

884 BC density and highlights the current assumption of a void-free structure of BC

885 particles in models would cause large uncertainties in CCN prediction and in the

886 relevant climate effect evaluation.

### 887 **Data availability.**

888 All data needed to evaluate the conclusions in the paper are present in the paper and/or

889 the Supplement. All data used in the study are also available from the corresponding

890 author upon request (zhangfang2021@hit.edu.cn).

删除了: 2

删除了: 4

删除了: currently

894 **Author contributions.**

895 FZ and JR conceived the conceptual development of the manuscript. JR directed and  
896 performed of the experiments with JL, LC, and FZ. JR conducted the data analysis and  
897 wrote the draft of the manuscript. All authors edited and commented on the various  
898 sections of the manuscript.

899 **Acknowledgments.**

900 This work was funded by the National Natural Science Foundation of China (NSFC)  
901 research project (41975174, 41675141). We thank all participants in the field campaigns  
902 for their tireless work and cooperation. We also thank Dr. Yele Sun and his group for  
903 providing the data of nonrefractory submicron aerosol chemical composition.

904 **Competing interests.**

905 The contact author has declared that neither they nor their co-authors have any  
906 competing interests.

907 **References**

908 Alfara, M. R., Paulsen, D., Gysel, M., Garforth, A. A., Dommen, J., Prévôt, A. S. H.,  
909 Worsnop, D. R., Baltensperger, U., and Coe, H.: A mass spectrometric study of  
910 secondary organic aerosols formed from the photooxidation of anthropogenic and  
911 biogenic precursors in a reaction chamber, *Atmos. Chem. Phys.*, 6, 5279– 5293,  
912 [https://doi:10.5194/acp-6-5279-2006](https://doi.org/10.5194/acp-6-5279-2006), 2006.  
913 Bond, T. C., Doherty, S. J., Fahey, D., Forster, P., Berntsen, T., DeAngelo, B., Flanner,  
914 M., Ghan, S., Kärcher, B., and Koch, D.: Bounding the role of black carbon in the

915 climate system: A scientific assessment, *J. Geophys. Res.-Atmos.*, 118(11), 5380–  
916 5552, <https://doi.org/10.1002/jgrd.50171>, 2013

917 Clarke, A.D., Shinozuka, Y., Kapustin, V.N., Howell, S., Huebert, B., Doherty, S.,  
918 Anderson, T., Covert, D., Anderson, J., Hua, X., Moore II, K.G., McNaughton, C.,  
919 Carmichael, G., Weber, R.: Size distributions and mixtures of dust and black carbon  
920 aerosol in Asian outflow: physiochemistry and optical properties, *J. Geophys. Res.-*  
921 *Atmos.*, 109, D15S09, <https://doi.org/10.1029/2003JD004378>, 2004.

922 Cheng, Y. F., Su, H., Rose, D., Gunthe, S. S., Berghof, M., Wehner, B., Achtert, P.,  
923 Nowak, A., Takegawa, N., Kondo, Y., Shiraiwa, M., Gong, Y. G., Shao, M., Hu, M.,  
924 Zhu, T., Zhang, Y. H., Carmichael, G. R., Wiedensohler, A., Andreae, M. O., and  
925 Pöschl, U.: Size-resolved measurement of the mixing state of soot in the megacity  
926 Beijing, China: diurnal cycle, aging and parameterization, *Atmos. Chem. Phys.*, 12,  
927 4477–4491, <https://doi.org/10.5194/acp-12-4477-2012>, 2012.

928 [Cheng, Y. F., Eichler, H., Wiedensohler, A., Heintzenberg, J., Zhang, Y. H., Hu, M.,](#)  
929 [Herrmann, H., Zeng, L. M., Liu, S., Gnauk, T., Brüggemann, E., and He, L. Y.:](#)  
930 [Mixing state of elemental carbon and non-light-absorbing aerosol components](#)  
931 [derived from in situ particle optical properties at Xinken in Pearl River Delta of China,](#)  
932 [J. Geophys. Res., 111, D20204, doi:10.1029/2005JD006929, 2006.](#)

933 Chen, L., F. Zhang, P. Yan, X. Wang, L. Sun, Y. Li, X. Zhang, Y. Sun, and Z. Li.: The  
934 large proportion of black carbon (BC)-containing aerosols in the urban atmosphere,  
935 *Environ. Pollut.*, 263, 114507, <https://doi.org/10.1016/j.envpol.2020.114507>, 2020.

936 Chang, R. Y.-W., Slowik, J. G., Shantz, N. C., Vlasenko, A., Liggio, J., Sjostedt, S. J.,  
937 Leaitch, W. R., and Abbatt, J. P. D.: The hygroscopicity parameter ( $k$ ) of ambient  
938 organic aerosol at a field site subject to biogenic and anthropogenic influences:  
939 relationship to degree of aerosol oxidation, *Atmos. Chem. Phys.*, 10, 5047–5064,  
940 <https://doi.org/10.5194/acp-10-5047-2010>, 2010.

941 [Cai, M., Tan, H., Chan, C. K., Qin, Y., Xu, H., Li, F., Schurman, M. I., Liu, L., and Zhao,](#)  
942 [J.: The size-resolved cloud condensation nuclei \(CCN\) activity and its prediction](#)  
943 [based on aerosol hygroscopicity and composition in the Pearl Delta River \(PRD\)](#)  
944 [region during wintertime 2014, Atmos. Chem. Phys., 18, 16419–16437,](#)  
945 [https://doi.org/10.5194/acp-18-16419-2018, 2018.](#)

946 [Dinar, E., Mentel, T. F., and Rudich, Y.: The density of humic acids and humic like](#)  
947 [substances \(HULIS\) from fresh and aged wood burning and pollution aerosol](#)  
948 [particles, Atmos. Chem. Phys., 6, 5213–5224, doi:10.5194/acp-6-5213-2006, 2006.](#)

949 Dameto de España, C., Wonauschütz, A., Steiner, G., Rosati, B., Demattio, A., Schuh,  
950 H., and Hitznerberger, R.: Long-term quantitative field study of New Particle  
951 Formation (NPF) events as a source of Cloud Condensation Nuclei (CCN) in the  
952 urban background of Vienna, *Atmos. Environ.*, 164, 289–298,  
953 <https://doi.org/10.1016/j.atmosenv.2017.06.001>, 2017.

954 Flanner, M. G., Zender, C. S., Randerson, J. T., and Rasch, P. J.: Present-day climate  
955 forcing and response from black carbon in snow, *J. Geophys. Res.-Atmos.*, 112,  
956 D11202, <https://doi.org/10.1029/2006JD008003>, 2007.

957 Fan, X., Liu, J., Zhang, F., Chen, L., Conllins, D., Xu, W., Jin, X., Ren, J., Wang, Y., Wu,  
958 H., Li, S., Sun, Y., Li, Z.: Contrasting size-resolved hygroscopicity of fine particles

959 derived by HTDMA and HR-ToF-AMS measurements between summer and winter  
960 in Beijing: the impacts of aerosol aging and local emissions, *Atmos. Chem. Phys.* 20,  
961 915-929, <https://doi.org/10.5194/acp-20-915-2020>, 2020.

962 Geller, M., Biswas, S., and Sioutas, C.: Determination of particle effective density in  
963 urban environments with a differential mobility analyzer and aerosol particle mass  
964 analyzer. *Aerosol Sci. Technol.*, 40, 709–723,  
965 <https://doi.org/10.1080/02786820600803925>, 2006.

966 Gysel, M., McFiggans, G. B., and Coe, H.: Inversion of tandem differential mobility  
967 analyser (TDMA) measurements, *J. Aerosol Sci.*, 40, 134–151,  
968 <https://doi.org/10.1016/j.jaerosci.2008.07.013>, 2009.

969 Gysel, M., Crosier, J., Topping, D. O., Whitehead, J. D., Bower, K. N., Cubison, M. J.,  
970 Williams, P. I., Flynn, M. J., McFiggans, G. B., and Coe, H.: Closure study between  
971 chemical composition and hygroscopic growth of aerosol particles during TORCH2,  
972 *Atmos. Chem. Phys.*, 7, 6131–6144, <https://doi.org/10.5194/acp-7-6131-2007>, 2007.

973 Gunthe, S. S., King, S. M., Rose, D., Chen, Q., Roldin, P., Farmer, D. K., Jimenez, J.  
974 L., Artaxo, P., Andreae, M. O., Martin, S. T., and Pöschl, U.: Cloud condensation  
975 nuclei in pristine tropical rainforest air of Amazonia: size resolved measurements and  
976 modeling of atmospheric aerosol composition and CCN activity, *Atmos. Chem. Phys.*,  
977 9, 7551–7575, <https://doi.org/10.5194/acp-9-7551-2009>, 2009.

978 Gysel, M., Laborde, M., Olfert, J. S., Subramanian, R., & Gröhn, A. J.: Effective density  
979 of aquadag and fullerene soot black carbon reference materials used for SP2  
980 calibration, *Atmos. Meas. Tech.*, 4(12), 4937–4955, [https://doi.org/10.5194/amt-4-](https://doi.org/10.5194/amt-4-2851-2011)  
981 [2851-2011](https://doi.org/10.5194/amt-4-2851-2011), 2011.

982 Gysel, M., Laborde, M., Mensah, A. A., Corbin, J. C., Keller, A., Kim, J., et al.:  
983 Technical note: The single particle soot photometer fails to reliably detect PALAS  
984 soot nanoparticles, *Atmos. Meas. Tech.*, 5(12), 3099–3107,  
985 <https://doi.org/10.5194/amt-5-3099-2012>, 2012.

986 Jimenez, J. L., Canagaratna, M. R., Donahue, N. M., Prevot, A. S. H., Zhang, Q., Kroll,  
987 J. H., DeCarlo, P. F., Allan, J. D., Coe, H., Ng, N. L., Aiken, A. C., Docherty, K. S.,  
988 Ulbrich, I. M., Grieshop, A. P., Robinson, A. L., Duplissy, J., Smith, J. D., Wilson,  
989 K. R., Lanz, V. A., Hueglin, C., Sun, Y. L., Tian, J., Laaksonen, A., Raatikainen, T.,  
990 Rautiainen, J., Vaattovaara, P., Ehn, M., Kulmala, M., Tomlinson, J. M., Collins, D.  
991 R., Cubison, M. J., Dunlea, E. J., Huffman, J. A., Onasch, T. B., Alfarra, M. R.,  
992 Williams, P. I., Bower, K., Kondo, Y., Schneider, J., Drewnick, F., Borrmann, S.,  
993 Weimer, S., Demerjian, K., Salcedo, D., Cottrell, L., Griffin, R., Takami, A., Miyoshi,  
994 T., Hatakeyama, S., Shimojo, A., Sun, J. Y., Zhang, Y. M., Dzepina, K., Kimmel, J.  
995 R., Sueper, D., Jayne, J. T., Herndon, S. C., Trimborn, A. M., Williams, L. R., Wood,  
996 E. C., Middlebrook, A. M., Kolb, C. E., Baltensperger, U., and Worsnop, D. R.:  
997 Evolution of Organic Aerosols in the Atmosphere, *Science*, 326, 1525–1529,  
998 <https://doi.org/10.1126/science.1180353>, 2009.

999 Kiselev, A., Wennrich, C., Stratmann, F., Wex, H., Henning, S., Mentel, T.F., Kiendler-  
1000 Scharr, A., Schneider, J., Walter, S., Lieberwirth, I.: Morphological characterization  
1001 of soot aerosol particles during LACIS Experiment in November (LExNo), *J.*  
1002 *Geophys. Res. -Atmos.*, 115, D11204, <https://doi.org/10.1029/2009jd012635>, 2010.

1003 Khalizov, A. F., Zhang, R., Zhang, D., Xue, H., Pagels, J., and McMurry, P. H.:  
1004 Formation of highly hygroscopic soot aerosols upon internal mixing with sulfuric  
1005 acid vapor, *J. Geophys. Res.-Atmos.*, 114, D05208,  
1006 <https://doi.org/10.1029/2008jd010595>, 2009.

1007 Kawana, K., Nakayama, T., and Mochida, M.: Hygroscopicity and CCN activity of  
1008 atmospheric aerosol particles and their relation to organics: Characteristics of urban  
1009 aerosols in Nagoya, Japan, *J. Geophys. Res.-Atmos.*, 121, 4100–4121,  
1010 <https://doi.org/10.1002/2015JD023213>, 2016.

1011 Li, M., Zhang, Q., Kurokawa, J.-I., Woo, J.-H., He, K., Lu, Z., Ohara, T., Song, Y.,  
1012 Streets, D. G., Carmichael, G. R., Cheng, Y., Hong, C., Huo, H., Jiang, X., Kang, S.,  
1013 Liu, F., Su, H., and Zheng, B.: MIX: a mosaic Asian anthropogenic emission  
1014 inventory under the international collaboration framework of the MICS-Asia and  
1015 HTAP, *Atmos. Chem. Phys.*, 17, 935–963, <https://doi.org/10.5194/acp-17-935-2017>,  
1016 2017.

1017 Liu, D., Joshi, R., Wang, J., Yu, C., Allan, J. D., Coe, H., Flynn, M. J., Xie, C., Lee, J.,  
1018 Squires, F., Kotthaus, S., Grimmond, S., Ge, X., Sun, Y., and Fu, P.: Contrasting  
1019 physical properties of black carbon in urban Beijing between winter and summer,  
1020 *Atmos. Chem. Phys.*, 19, 6749–6769, <https://doi.org/10.5194/acp-19-6749-2019>,  
1021 [2019a](#).

1022 Liu, D., Allan, J., Whitehead, J., Young, D., Flynn, M., Coe, H., McFiggans, G.,  
1023 Fleming, Z. L., and Bandy, B.: Ambient black carbon particle hygroscopic properties  
1024 controlled by mixing state and composition, *Atmos. Chem. Phys.*, 13, 2015–2029,  
1025 <https://doi.org/10.5194/acp-13-2015-2013>, 2013.

1026 Liu, H., Pan, X.L., Wu, Y., Wang, D.W., Tian, Y., Liu, X.Y., et al.: Effective densities of  
1027 soot particles and their relationships with the mixing state at an urban site in the  
1028 Beijing megacity in the winter of 2018, *Atmos. Chem. Phys.* 19, 14791–14804,  
1029 <https://doi.org/10.5194/acp-19-14791-2019>, [2019b](#).

1030 Lide, D. R. (ed.). *CRC Handbook of Chemistry and Physics*. CRC Press: Ann Arbor,  
1031 MI. (1992).

1032 Lance, S., Medina, J., Smith, J., and Nenes, A.: Mapping the operation of the DMT  
1033 continuous flow CCN counter, *Aerosol Sci. Tech.*, 40, 242–254,  
1034 <https://doi.org/10.1080/02786820500543290>, 2006.

1035 Liu, H., Pan, X., Liu, D., Liu, X., Chen, X., Tian, Y., Sun, Y., Fu, P., and Wang, Z.:  
1036 Mixing characteristics of refractory black carbon aerosols at an urban site in Beijing,  
1037 *Atmos. Chem. Phys.*, 20, 5771–5785, <https://doi.org/10.5194/acp-20-5771-2020>,  
1038 2020.

1039 Liu, L., Zhang, J, Zhang, Y, Wang, Y, Xu, L, Yuan, Q, et al.: Persistent residential  
1040 burning-related primary organic particles during wintertime hazes in North China:  
1041 insights into their aging and optical changes, *Atmos. Chem. Phys.* 21, 2251–2265,  
1042 <https://doi.org/10.5194/acp-21-2251-2021>, [2021a](#).

1043 [Liu, J., Zhang, F., Xu, W., Sun, Y., Chen, L., Li, S.: Hygroscopicity of organic aerosols](#)  
1044 [linked to formation mechanisms. \*Geophysical Research Letters\*. 48, e2020GL091683.](#)  
1045 <https://doi.org/10.1029/2020gl091683>, [2021b](#).

1046 McMurry, H. Peter, Wang Xin, Park Kihong & Ehara Kensei.: The Relationship

删除了: 2019

删除了: 2019

删除了: 2021



1050 between Mass and Mobility for Atmospheric Particles: A New Technique for  
1051 Measuring Particle Density, *Aerosol Sci. Technol.*, 36:2, 227-238,  
1052 <https://doi.10.1080/027868202753504083>, 2002.

1053 Massoli, P., Onasch, T.B., Cappa, C.D., Nuamaan, I., Hakala, J., Hayden, K., Li, S.M.,  
1054 Sueper, D.T., Bates, T.S., Quinn, P.K., Jayne, J.T., Worsnop, D.R.: Characterization  
1055 of black carbon-containing particles from soot particle aerosol mass spectrometer  
1056 measurements on the R/V Atlantis during CalNex 2010, *J. Geophys. Res.- Atmos.*,  
1057 120, 2575-2593, <https://doi.org/10.1002/2014JD022834>, 2015.

1058 Mei, F., Setyan, A., Zhang, Q., and Wang, J.: CCN activity of organic aerosols observed  
1059 downwind of urban emissions during CARES, *Atmos. Chem. Phys.*, 13, 12155–  
1060 12169, <https://doi.org/10.5194/acp-13-12155-2013>, 2013.

1061 [Meng, J. W., Yeung, M. C., Li, Y. J., Lee, B. Y. L., and Chan, C. K.: Size-resolved cloud](https://doi.org/10.5194/acp-14-10267-2014)  
1062 [condensation nuclei \(CCN\) activity and closure analysis at the HKUST Supersite in](https://doi.org/10.5194/acp-14-10267-2014)  
1063 [Hong Kong, \*Atmos. Chem. Phys.\*, 14, 10267–10282, \[https://doi.org/10.5194/acp-14-\]\(https://doi.org/10.5194/acp-14-10267-2014\)](https://doi.org/10.5194/acp-14-10267-2014)  
1064 [10267-2014, 2014.](https://doi.org/10.5194/acp-14-10267-2014)

1065 Noureddini, H., Teoh, B. C., Davis Clements, L.: Densities of vegetable oils and fatty  
1066 acids, *J. Am. Oil Chem. Soc.*, 69 (12), 1184–1188, 1992.

1067 Olfert, J. S., Symonds, J. P. R., and Collings, N.: The effective density and fractal  
1068 dimension of particles emitted from a light-duty diesel vehicle with a diesel oxidation  
1069 catalyst, *J. Aerosol Sci.*, 38, 69–82, <https://doi.org/10.1016/j.jaerosci.2006.10.002>,  
1070 2007.

1071 Park, K., Kittelson, D. B., and McMurry, P. H.: Structural properties of diesel exhaust  
1072 particles measured by transmission electron microscopy (TEM): Relationships to  
1073 particle mass and mobility, *Aerosol Sci. Technol.*, 38, 881–889,  
1074 <https://doi.org/10.1080/027868290505189>, 2004.

1075 Pagels, J., Khalizov, A.F., McMurry, P.H. and Zhang, R.Y.: Processing of soot by  
1076 controlled sulphuric acid and water condensation-mass and mobility relationship,  
1077 *Aerosol Sci. Technol.*, 43, 629–640, <https://doi.org/10.1080/02786820902810685>,  
1078 2009.

1079 Peng, J. F., Hu, M., Guo, S., Du, Z. F., Zheng, J., Shang, D. J., Zamora, M., Zeng, L.  
1080 M., Shao, M., Wu, Y. S., Zheng, J., Wang, Y., Glen, C., Collins, D., Molina, M., and  
1081 Zhang, R. Y.: Markedly enhanced absorption, and direct radiative forcing of black  
1082 carbon under polluted urban environments, *P. Natl. Acad. Sci. USA*, 113(16), 4266–  
1083 4271, <https://doi.org/10.1073/pnas.1602310113>, 2016.

1084 Petters, M. D. and Kreidenweis, S. M.: A single parameter representation of  
1085 hygroscopic growth and cloud condensation nucleus activity, *Atmos. Chem. Phys.*,  
1086 7, 1961–1971, <https://doi.org/10.5194/acp-7-1961-2007>, 2007.

1087 Paatero, P. and Tapper, U.: Positive matrix factorization: A nonnegative factormodel  
1088 with optimal utilization of error estimates of data values, *Environmetrics*, 5, 111–126,  
1089 1994.

1090 Peng, J. F., Hu, M., Guo, S., Du, Z. F., Zheng, J., M., Zeng, L. M., Shao, M., Wu, Y. S.,  
1091 Collins, D., Molina, M., and Zhang, R. Y.: Ageing and hygroscopicity variation of  
1092 black carbon particles in Beijing measured by a quasi-atmospheric aerosol evolution

1093 study (QUALITY) chamber, *Atmos. Chem. Phys.*, 17(17), 10333-10348,  
1094 <https://doi.org/10.5194/acp-17-10333-2017>, 2017.

1095 Pan, X.L., Kanaya, Y., Taketani, F., Miyakawa, T., Inomata, S., Komazaki, Y., et al.:  
1096 Emission characteristics of refractory black carbon aerosols from fresh biomass  
1097 burning: a perspective from laboratory experiments, *Atmos. Chem. Phys.*, 17(21),  
1098 13001–13016, <https://doi.org/10.5194/acp-17-13001-2017>, 2017.

1099 Park, K., Cao, F., Kittelson, D. B., & McMurry, P. H.: Relationship between particle  
1100 mass and mobility for diesel exhaust particles, *Environ. Sci. Technol.*, 37, 577–583,  
1101 <https://doi.org/10.1021/es025960v>, 2003.

1102 Qiao, K., Wu, Z., Pei, X., Liu, Q., Shang, D., Zheng, J., Du, Z., Zhu, W., Wu, Y., Lou, S.,  
1103 Guo, S., Chan, C.K., Pathak, R.K., Hallquist, M., Hu, M.: Size-resolved effective  
1104 density of submicron particles during summertime in the rural atmosphere of Beijing,  
1105 China, *J. Environ. Sci. (China)* 73, 69–77. <https://doi.org/10.1016/j.jes.2018.01.012>,  
1106 2018.

1107 Rissler, J., Nordin, E. Z., Eriksson, A. C., Nilsson, P. T., Frosch, M., Sporre, M. K.,  
1108 Wierzbicka, A., Svenningsson, B., Londahl, J., Messing, M. E., Sjogren, S.,  
1109 Hemmingsen, J. G., Loft, S., Pagels, J. H., and Swietlicki, E.: Effective Density and  
1110 Mixing State of Aerosol Particles in a Near-Traffic Urban Environment, *Environ. Sci.*  
1111 *Technol.*, 48, 6300–6308, <https://doi.org/10.1021/es5000353>, 2014.

1112 Riemer, N., Vogel, H., and Vogel, B.: Soot aging time scales in polluted regions during  
1113 day and night, *Atmos. Chem. Phys.*, 4, 1885–1893, [https://doi.org/10.5194/acp-4-](https://doi.org/10.5194/acp-4-1885-2004)  
1114 [1885-2004](https://doi.org/10.5194/acp-4-1885-2004), 2004.

1115 Ramanathan, V. and Carmichael, G.: Global and regional climate changes due to black  
1116 carbon, *Nat. Geosci.*, 36, 221-227, <https://doi.org/10.1038/ngeo156>, 2008.

1117 Ren, J., Zhang, F., Wang, Y., Collins, D., Fan, X., Jin, X., et al.: Using different  
1118 assumptions of aerosol mixing state and chemical composition to predict CCN  
1119 concentrations based on field measurements in urban Beijing, *Atmos. Chem. Phys.*,  
1120 18, 6907–6921, <https://doi.org/10.5194/acp-18-6907-2018>, 2018.

1121 Rader, D.J., McMurry, P.H.: Application of the tandem differential mobility analyzer  
1122 to studies of droplet growth or evaporation, *J. Geophys. Res.- Atmos.*, 17, 771-787,  
1123 [https://doi.org/10.1016/0021-8502\(86\)90031-5](https://doi.org/10.1016/0021-8502(86)90031-5), 1986.

1124 Reyes-Villegas, E., Bannan, T., Le Breton, M., Mehra, A., Priestley, M., Percival, C.,  
1125 Coe, H., and Allan, J. D.: Online Chemical Characterization of Food-Cooking  
1126 Organic Aerosols: Implications for Source Apportionment, *Environ. Sci. Technol.*,  
1127 52, 5308–5318, <https://doi.org/10.1021/acs.est.7b06278>, 2018.

1128 Schwarz, J. P., Gao, R. S., Spackman, J. R., Watts, L. A., Thomson, D. S., Fahey, D.  
1129 W., Ryerson, T. B., Peischl, J., Holloway, J. S., Trainer, M., Frost, G. J., Baynard,  
1130 T., Lack, D. A., de Gouw, J. A., Warneke, C., and Del Negro, L. A.: Measurement  
1131 of the mixing state, mass, and optical size of individual black carbon particles in  
1132 urban and biomass burning emissions, *Geophys. Res. Lett.*, 35, L13810,  
1133 <https://doi.org/10.1029/2008GL033968>, 2008.

1134 Stokes, R. and Robinson, R.: Interactions in aqueous nonelectrolyte solutions, I. Solute-  
1135 solvent equilibria, *J. Phys. Chem.-US*, 70, 2126–2131, 1966.

1136 Sun, Y., Du, W., Fu, P., Wang, Q., Li, J., Ge, X., Zhang, Q., Zhu, C., Ren, L., Xu, W.,

1137 Zhao, J., Han, T., Worsnop, D. R., and Wang, Z.: Primary, and secondary aerosols  
1138 in Beijing in winter: sources, variations, and processes, *Atmos. Chem. Phys.*, 16,  
1139 8309–8329, <https://doi.org/10.5194/acp-16-8309-2016>, 2016.

1140 Sun, Y. L., Wang, Z. F., Du, W., Zhang, Q., Wang, Q. Q., Fu, P. Q., Pan, X. L., Li, J.,  
1141 Jayne, J., and Worsnop, D. R.: Long term real-time measurements of aerosol particle  
1142 composition in Beijing, China: seasonal variations, meteorological effects, and  
1143 source analysis, *Atmos. Chem. Phys.*, 15, 10149–10165, <https://doi.org/10.5194/acp-15-10149-2015>, 2015.

1145 Shiraiwa, M., Kondo, Y., Moteki, N., Takegawa, N., Sahu, L., Takami, A., et al.:  
1146 Radiative impact of mixing state of black carbon aerosol in Asian outflow, *J.*  
1147 *Geophys. Res.- Atmos.*, 113, D24210, <https://doi.org/10.1029/2008JD010546>, 2008.

1148 Tan, H., Xu, H., Wan, Q., Li, F., Deng, X., Chan, P. W., Xia, D., and Yin, Y.: Design  
1149 and application of an unattended multifunctional H-TDMA system, *J. Atmos. Ocean.*  
1150 *Tech.*, 30, 1136–1148, <https://doi.org/10.1175/JTECH-D-12-00129.1>, 2013.

1151 Ulbrich, I. M., Canagaratna, M. R., Zhang, Q., Worsnop, D. R., and Jimenez, J. L.:  
1152 Interpretation of organic components from Positive Matrix Factorization of aerosol  
1153 mass spectrometric data, *Atmos. Chem. Phys.*, 9, 2891–2918,  
1154 <https://doi.org/10.5194/acp-9-2891-2009>, 2009.

1155 Wang, Y., Wan, Q., Meng, W., Liao, F., Tan, H., and Zhang, R.: Long-term impacts of  
1156 aerosols on precipitation and lightning over the Pearl River Delta megacity area in  
1157 China, *Atmos. Chem. Phys.*, 11, 12421–12436, <https://doi.org/10.5194/acp-11-12421-2011>, 2011.

1159 Wang, Y. Y., Liu, F. S., He, C. L., Bi, L., Cheng, T. H., Wang, Z. L., Zhang, H., Zhang,  
1160 X. Y., Shi, Z. B., and Li, W. J.: Fractal dimensions and mixing structures of soot  
1161 particles during atmospheric processing, *Environ. Sci. Tech. Lett.*, 4, 487–493,  
1162 <https://doi.org/10.1021/acs.estlett.7b00418>, 2017.

1163 Wu, Y. F., Xia, Y. J., Huang, R. J., Deng, Z. Z., Tian, P., Xia, X. G., et al.: A study of the  
1164 morphology and effective density of externally mixed black carbon aerosols in  
1165 ambient air using a size-resolved single-particle soot photometer (SP2), *Atmos. Meas.*  
1166 *Tech.*, 12, 4347–4359, <https://doi.org/10.5194/amt-12-4347-2019>, 2019.

1167 Wu, Y., Wang, X., Tao, J., Huang, R., Tian, P., Cao, J., Zhang, L., Ho, K.-F., Han, Z.,  
1168 and Zhang, R.: Size distribution and source of black carbon aerosol in urban Beijing  
1169 during winter haze episodes, *Atmos. Chem. Phys.*, 17, 7965–7975,  
1170 <https://doi.org/10.5194/acp-17-7965-2017>, 2017.

1171 Wu, Z. J., Zheng, J., Shang, D. J., Du, Z. F., Wu, Y. S., Zeng, L. M., Wiedensohler, A.,  
1172 and Hu, M.: Particle hygroscopicity and its link to chemical composition in the urban  
1173 atmosphere of Beijing, China, during summertime, *Atmos. Chem. Phys.*, 16, 1123–  
1174 1138, <https://doi.org/10.5194/acp-16-1123-2016>, 2016.

1175 Xue, H., Khalizov, A. F., Wang, L., Zheng, J., and Zhang, R.: Effects of dicarboxylic  
1176 acid coating on the optical properties of soot, *Phys. Chem. Chem. Phys.*, 11, 7869–  
1177 7875, <https://doi.org/10.1039/b904129j>, 2009.

1178 Xu, W., Sun, Y., Wang, Q., Zhao, J., Wang, J., Ge, X., et al.: Changes in aerosol  
1179 chemistry from 2014 to 2016 in winter in Beijing: Insights from high-resolution  
1180 aerosol mass spectrometry, *J. Geophys. Res.-Atmos.*, 124, 1132–1147.

1181 <https://doi.org/10.1029/2018jd029245>, 2019.

1182 Xu, W., Fossom, K. N., Ovadnevaite, J., Lin, C., Huang, R.-J., O'Dowd, C., and

1183 Ceburnis, D.: The impact of aerosol size-dependent hygroscopicity and mixing state

1184 on the cloud condensation nuclei potential over the north-east Atlantic, *Atmos. Chem.*

1185 *Phys.*, 21, 8655–8675, <https://doi.org/10.5194/acp-21-8655-2021>, 2021.

1186 Yuan, T., Li, Z., Zhang, R., and Fan, J.: Increase of cloud droplet size with aerosol

1187 optical depth: An observation and modeling study, *J. Geophys. Res.-Atmos.*, 113,

1188 D04201, <https://doi.org/10.1029/2007JD008632>, 2008.

1189 Yu, C., Liu, D., Broda, K., Joshi, R., Olfert, J., Sun, Y., Fu, P., Coe, H., Allan, J.D.:

1190 Characterising mass-resolved mixing state of black carbon in Beijing using a

1191 morphology-independent measurement method, *Atmos. Chem. Phys.*, 20, 3645–

1192 3661. <https://doi.org/10.5194/acp-20-3645-2020>, 2020.

1193 Zhang, R. Y., Khalizov, A. F., Pagels, J., Zhang, D., Xue, H. X., and McMurry, P. H.:

1194 Variability in morphology, hygroscopicity, and optical properties of soot aerosols

1195 during atmospheric processing, *P. Natl. Acad. Sci. USA*, 105, 10291–10296,

1196 <https://doi.org/10.1073/pnas.0804860105>, 2008.

1197 Zhang, Y., Zhang, Q., Cheng, Y., Su, H., Kecorius, S., Wang, Z., Wu, Z., Hu, M., Zhu,

1198 T., Wiedensohler, A., and He, K.: Measuring the morphology and density of

1199 internally mixed black carbon with SP2 and VTDMA: new insight into the

1200 absorption enhancement of black carbon in the atmosphere, *Atmos. Meas. Tech.*, 9,

1201 1833–1843, <https://doi.org/10.5194/amt-9-1833-2016>, 2016.

1202 Zdanovskii, A.: New methods for calculating solubilities of electrolytes in

1203 multicomponent systems, *Zh. Fiz. Khim.C*, 22, 1475– 1485, 1948.

1204 Zhang, F., Wang, Y., Peng, J., Ren, J., Collins, D., Zhang, R., et al.: Uncertainty in

1205 predicting CCN activity of aged and primary aerosols, *J. Geophys. Res.-Atmos.*,

1206 122(21), 11723–11736, <https://doi.org/10.1002/2017jd027058>, 2017.

1207 Zhang, F., Ren, J., Fan, T., Chen, L., Xu, W., Sun, Y., et al.: Significantly enhanced

1208 aerosol CCN activity and number, *J. Geophys. Res.-Atmos.*, 124, 14102–14113,

1209 <https://doi.org/10.1029/2019jd031457>, 2019.

1210 Zhang, F., Wang, Y., Peng, J., Chen, L., Sun, Y., Duan, L., Ge, X., Li, Y., Zhao, J., Liu,

1211 C., Zhang, X., Zhang, G., Pan, Y., Wang, Y., Zhang, A. L., Ji, Y., Wang, G., Hu, M.,

1212 Molina, M. J., Zhang, R.: An unexpected catalyst dominates formation and radiative

1213 forcing of regional haze, *P. Natl. Acad. Sci. USA*, 117(8), 3960–3966,

1214 <https://doi.org/10.1073/pnas.1919343117>, 2020a.

1215 Zhang, Y., Zhang, Q., Yao, Z., Li, H.: Particle Size and Mixing State of Freshly Emitted

1216 Black Carbon from Different Combustion Sources in China, *Environ. Sci. Technol.*,

1217 54(13): p. 7766-7774, <https://doi.org/10.1021/acs.est.9b07373>, 2020b.

1218 Zhang, F., Peng, J., Chen, L., Collins, D., Li, Y., Jiang, S., Liu, J., Zhang, R.: The effect

1219 of Black carbon aging from NO<sub>2</sub> oxidation of SO<sub>2</sub> on its morphology, optical and

1220 hygroscopic properties, *Environ. Res.*, 212, 113238,

1221 <https://doi.org/10.1016/j.envres.2022.113238>, 2022.

1222 Zhang, R., Wang, G., Guo, S., Zamora, M. L., Ying, Q., Lin, Y.: Formation of urban

1223 fine particulate matter, *Chemical Reviews*, 115(10), 3803–3855,

1224 <https://doi.org/10.1021/acs.chemrev.5b00067>, 2015.

1225 Zhou, Y., Ma, N., Wang, Q., Wang, Z., Chen, C., Tao, J., Hong, J., Peng, L., He, Y.,

移动了(插入) [9]

下移了 [10]: Y., Zhang, Q., Yao, Z., Li, H.: Particle Size and Mixing State of Freshly Emitted Black Carbon from Different Combustion Sources in China, *Environ. Sci. Technol.*, 54(13): p. 7766-7774, <https://doi.org/10.1021/acs.est.9b07373>,

删除了: 2020

域代码已更改

上移了 [9]: F., Wang, Y., Peng, J., Ren, J., Collins, D., Zhang, R., et al.: Uncertainty in predicting CCN activity of aged and primary aerosols, *J. Geophys. Res.-Atmos.*, 122(21), 11723–11736, <https://doi.org/10.1002/2017jd027058>, 2017

删除了: Zhang,

删除了: .

删除了: 2020

移动了(插入) [10]

域代码已更改

删除了: Zhou, Y.,

1243 Xie, L., Zhu, S., Zhang, Y., Li, G., Xu, W., et al.: Bimodal distribution of size-  
1244 resolved particle effective density: results from a short campaign in a rural environ-  
1245 ment over the North China Plain, *Atmos. Chem. Phys.*, **22**, 2029–2047.  
1246 <https://doi.org/10.5194/acp-22-2029-2022>, 2022.

1247 Zhao, G., Tan, T., Hu, S., Du, Z., Shang, D., Wu, Z., Guo, S., Zheng, J., Zhu, W., Li,  
1248 M., Zeng, L., and Hu, M.: Mixing state of black carbon at different atmospheres in  
1249 north and southwest China, *Atmos. Chem. Phys.*, **22**, 10861–10873,  
1250 <https://doi.org/10.5194/acp-22-10861-2022>, 2022.